ELSEVIER

Contents lists available at ScienceDirect

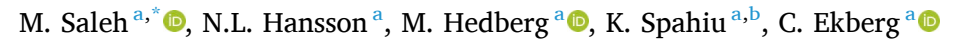
## Journal of Nuclear Materials

journal homepage: www.elsevier.com/locate/jnucmat



## Review

## Dissolution of unirradiated MOX fuel in the presence of metallic iron





<sup>&</sup>lt;sup>b</sup> Swedish Nuclear Fuel and Waste Management Co., SE-101 24 Stockholm, Sweden

## HIGHLIGHTS

- Anoxic iron corrosion products neutralized the high alpha field of the MOX pellet.
- No oxidized uranium species were detected during 407 days of the leaching testing.
- Hydrogen gas was continuously produced, reaching ~2 bars at test termination.
- Uranium sorbed mainly onto iron corrosion products rather than vessel surfaces.
- Ankerite and chukanovite were identified as anoxic iron corrosion products, while several Fe(III) compounds including goethite, lepidocrocite and akageneite were
  formed on the surface of the MOX pellet.
- The anoxic iron corrosion in granitic groundwater completely inhibited MOX oxidative dissolution.

## ARTICLE INFO

# Keywords: MOX fuel Alpha radiolysis Iron Fuel dissolution Groundwater Anoxic corrosion

## ABSTRACT

In all European deep repository concepts for spent nuclear fuel, massive canisters made of or containing large amounts of iron are designed to prevent any early spent fuel contact with groundwater. In the case of canister failure, the corrosion of spent nuclear fuel will occur at repository depth, several hundred meters underground, where the groundwaters are typically anoxic. Spent nuclear fuel corrosion is therefore expected to occur simultaneously with anoxic iron corrosion. In this study the corrosion of an unirradiated MOX fuel pellet containing 10 wt % Pu (specific alpha activity 1.79 GBq/g) was investigated under Ar atmosphere in carbonated water (2 mM NaHCO<sub>3</sub>, 10 mM NaCl) and in simulated granitic groundwater from Forsmark, Sweden in the presence of metallic iron foils and iron powder. The anoxic conditions were simulated by degassing the solutions and by carrying out the tests in an autoclave pressurized with argon. The results of the test show that the anoxic corrosion products of iron neutralized completely the high alpha field of the MOX pellet. The production of hydrogen continued during the whole test with a linear rate of 8.5 10<sup>-5</sup> mol H<sub>2</sub>/day, reaching about 2 bars H<sub>2</sub> pressure at test termination. The Fe(II) concentrations increased from 5.6 10<sup>-4</sup> M after 101 days and MOX pellet insertion to 9.2 10<sup>-4</sup> M at test termination. No traces of oxidized uranium were observed in the autoclave during the whole duration (407 days) of the test; the uranium concentrations (from 2.9 10<sup>-9</sup> M at start to 1.2 10<sup>-9</sup> at the end) are in good agreement with the lower range of UO2(am) solubility. Massive Fe(III) precipitation was observed on the surface of the MOX pellet, but not in the bulk solution. The Pu concentrations were below the detection limit of alpha spectrometry. We have reported very low Pu concentrations only at the initial stage of the leaching as determined by ICP-MS, later Pu was under detection limit. The analysis of the iron foils, iron powder and vessel surfaces showed that the majority of U(IV) was sorbed on iron corrosion products and much less in the glass surfaces of the vessel. Anoxic iron corrosion products such as ankerite and probably chukanovite were detected on the iron foils, while several Fe(III) compounds including goethite, lepidocrocite and akageneite were formed on the surface of the MOX pellet. This study shows that the anoxic corrosion of iron in granitic Forsmark groundwaters completely inhibits the oxidative dissolution of a MOX pellet with a very high specific alpha activity.

E-mail address: gidam@chalmers.se (M. Saleh).

<sup>\*</sup> Corresponding author.

#### 1. Introduction

The dissolution rate of the  $UO_2$  fuel matrix is a key parameter in the safety assessment of a deep repository for spent nuclear fuel. The dissolution of the fuel matrix controls a large part of the radionuclide release to the groundwater in the event of a canister breach [1].  $UO_2$ -based spent nuclear fuel consists of approximately 95 %  $UO_2(s)$ ; the remaining 5 % are fission products and actinides.

The groundwater for most of the deep repository concepts is generally reducing and under such conditions,  $UO_2(s)$  is stable and has a very low solubility [2]. However, the groundwater adjacent to the spent fuel will be exposed to ionizing radiation due to the inherent radioactivity of the fission products and heavier actinides contained in the spent fuel. This will alter the redox conditions near the fuel surface due to the radiolysis of water. In this process, both radical and molecular oxidizing  $(OH\cdot, HO_2\cdot, H_2O_2 \text{ and } O_2)$  and reducing  $(e_{aq}^i, H\cdot \text{ and } H_2)$  species are produced [3]. The oxidants will oxidize U(IV) of the fuel matrix, or in the solution, to the significantly more soluble U(VI) and will thereby considerably enhance the rate of  $UO_2$ -matrix oxidative dissolution. Although oxidizing and reducing species are produced in equivalent amounts during radiolysis of water, the lower reactivity of the molecular reducing species,  $H_2$ , will lead to locally oxidizing conditions near the fuel surface.

In the Swedish and Finnish concepts for disposal of high-level waste, the spent nuclear fuel will be encapsulated in copper canisters with a massive cast-iron insert. In the case of a limited canister defect, the anoxic corrosion of iron gives rise to the production of hydrogen at a higher rate than its diffusive mass transport away from the canister. The groundwater inside the canister is expected to quickly become saturated with  $H_2$  [4,5].

In all geologic repository concepts, massive canisters assure that the spent nuclear fuel is not expected to be exposed to groundwater before storage times of the order of several thousand years have elapsed. The decay of fission products and actinides will result in the disappearance of short-lived radionuclides, which account for almost all the  $\beta\text{-}$  and  $\gamma\text{-}decays$  dominating the activity of the "young" spent fuel available today. As a result,  $\alpha\text{-}radiation$  will dominate the radiation field of the spent nuclear fuel already after a few hundred years of storage. Alpha radiation is a high LET (Linear Energy Transfer) radiation and produces mainly molecular radiolysis products, such as hydrogen peroxide and hydrogen.

A convenient way to obtain high specific  $\alpha$ -activity in the uranium dioxide matrix is to use un-irradiated MOX fuel with a relatively high Pucontent. Industrial MOX pellets present however heterogeneity in the Pu distribution that should be taken into account. The doping of UO2 with Pu (or other tetravalent cations, e.g. Th and Zr, which cannot be oxidized to a higher state) increases the stability of the solid towards oxidative dissolution, as shown by studies of unirradiated [6,7] or irradiated MOX fuel [8]. Leaching studies on un-irradiated MOX pellets, while interesting as highly α-doped UO<sub>2</sub> samples, remain also relevant in the context of long-term disposal of spent MOX fuel, an issue being faced by several countries. Although no clear scenario exists today for the ultimate fate of irradiated MOX fuel, the alternatives to direct disposal face serious hurdles. Multi-recycling for LWR fuel has been shown to be possible but is limited by the loss of reactivity caused by the build-up of non-fissile Pu isotopes. As a consequence of the mono-recycling limitation for MOX fuel, basically two routes are considered for the back end of spent MOX assemblies: further reprocessing and use as energy source in future reactor types, or direct disposal as waste in a final repository.

In the present work, an industrially produced un-irradiated MOX pellet with a high specific  $\alpha$ -activity was investigated through leaching experiments under Ar atmosphere in carbonated water (10 mM NaCl, 2 mM NaHCO $_3$ ) and in the presence of metallic iron in simulated Forsmark groundwater, containing Ca, Mg and other typical groundwater components.

During several spent fuel leaching and other tests involving solid

UO<sub>2</sub>, a simplified groundwater composition called "10:2 solution" (10 mM NaCl, 2 mM NaHCO<sub>3</sub>) with similar carbonate concentrations and ionic strength as granitic groundwater has been used by our group. The reasoning behind was to avoid groundwater cations (such as Ca and Mg) and silicate anions reported to hinder fuel dissolution or cause formation of very insoluble U(VI) solids. The concentrations of Fe(II) measured in tests with corroding iron and spent fuel in such simplified solutions were quite low ( $\sim 10^{-5}$  M) and the identified corrosion product was magnetite [9,10]. Similarly, Cui and Spahiu [11] reported Fe(II) concentrations in contact with corroding cast iron or carbon steel of 0.53-1.9 10<sup>-5</sup> M and carbonate green rust was identified as a corrosion product. In some recent tests carried out in our group with simulated Forsmark groundwaters, containing Ca and other groundwater components used in testing reductive precipitation of U(VI) on metallic iron surfaces [12], high Fe(II) concentrations were measured, in the range  $10^{-4}$  -  $10^{-3}$  M, quite similar to these measured with corroding iron and Callovo-Oxfordian groundwater [13-15]. For this reason, we chose to test the influence of corroding iron with highly active 10 wt % Pu MOX pellets in Forsmark groundwater containing Ca, Mg and other components of the groundwater.

The anoxic aqueous corrosion of iron may result in several corrosion products (green rust, chukanovite, ankerite, magnetite) depending on the redox conditions and the composition of the groundwater. Under strictly reducing conditions Fe(II)-hydroxide, Fe(OH)<sub>2</sub> initially forms, while in carbonate containing systems the Fe(II) minerals such as siderite (FeCO<sub>3</sub>) and chukanovite (Fe<sub>2</sub>(OH)<sub>2</sub>CO<sub>3</sub>) [16] are candidates. In less reducing or alternating redox conditions green rusts with Fe(II)/Fe (III) ratios of  $\sim$ 3–2 composed of a double layered structure with either CO<sub>3</sub><sup>2-</sup>, Cl<sup>-</sup> or SO<sub>4</sub><sup>2-</sup> anions may form [17,18]. The magnetite has been shown as the major anoxic iron corrosion product formed in granitic groundwaters in the long term [19–22]. Anoxic iron corrosion will lead to formation of dissolved Fe(II) and H<sub>2</sub>, both acting as repository reductants. Fe(II) and H<sub>2</sub> as reducing species can interact with the radiolytic oxidants from the fuel thereby influencing the fuel's corrosion behavior [9]:

$$Fe(s) + 2H_2O \rightarrow Fe^{2+} + 2OH^- + H_2(g)$$
 (1)

$$3Fe(s) + 4H_2O \rightarrow Fe_3O_4(s) + 4H_2(g)$$
 (2)

Previous studies have shown a significant impact of Fe(II) produced by iron corrosion in preventing the oxidative dissolution of spent nuclear fuel. Odorowski et al. [13] investigated highly doped UO $_2$  pellets (385 MBq/g) in simulated Callovo-Oxfordian groundwater and in the presence of metallic Fe foil under Ar atmosphere. The results of the more than one-year long test showed very low uranium concentrations in solution (ranging from  $4.10^{-9}$  -  $4.10^{-10}$  M), corresponding to the solubility of UO $_2$ ·xH $_2$ O. The authors concluded that Fe(II) produced by iron corrosion completely cancels the oxidative dissolution of the highly doped pellets. Similar results were reported in [14,15] for the leaching of an unirradiated MOX pellet with alpha activity  $1.3\times10^9$  Bq/g, in the presence of iron foils. The strong effect of Fe(II) observed in these tests is probably due to formation of hydroxo-carbonates as Fe corrosion products, leading to relatively high measured Fe(II) concentrations  $(10^{-4}$  -  $10^{-3}$  M) in solution.

The primary objective of this study is to investigate the dissolution behavior of unirradiated MOX fuel in the presence of metallic iron, under conditions simulating a deep geological repository in granitic bedrock. To simulate such conditions, a MOX fuel pellets with high specific activity was used in this study. This choice of fuel is justified by its simplicity and cost-effectiveness. It has been shown in several studies that iron corroding in Callovo-Oxfordian groundwater counteracts successfully very high alpha doses originating from pellets with up to 24 % Pu. The main objective of this study was to show that even for the composition of the Forsmark granitic groundwater, the corrosion of metallic iron creates redox conditions inside the canister that can counteract the high alpha radiation field of the unirradiated MOX pellet

containing 10 wt % Pu.

## 2. Materials and methods

## 2.1. Materials

## 2.1.1. Unirradiated MIMAS-MOX fuel

A 10 wt. % Pu unirradiated MOX pellet, produced in the MELOX factory in Marcoule, France through the MIMAS (MIcronized MASterblend)-MOX process was used in these experiments. The pellet was manufactured with a density of  $\sim\!95\,\%$  of the theoretical density and had a specific alpha-activity of 1.71 GBq/g. The pellet used in these experiments was a subdivided piece of the initial MIMAS-MOX pellet produced by cutting the original pellet in two slices. The slice used in this study had a mass of 1.6657 g and cylindrical geometry. The composition of the pellet is shown in Table 1. The pellet was used in the simplified 10:2 solution under Ar atmosphere in tests starting June 2019 then used again after annealing in granitic groundwater in the presence of iron with start August 2023.

MIMAS-MOX fuel has a heterogeneous microstructure, with three separate zones containing varying degrees of Pu concentrations, originating from the production process (dilution of a  $\rm UO_2$  and  $\rm PuO_2$  master blend with  $\rm UO_2$  powder) and the origin of the  $\rm UO_2$  powder used [22]. For the 7.48 % Pu MIMAS-MOX pellet investigated in [6], these three zones comprise:

- a UO<sub>2</sub> matrix containing around 2.7 hma % (heavy metal atom percent) Pu, which corresponds to about 15wt % of the total Pu.
- Pu rich agglomerates containing around 20.2 hma % Pu, corresponding to 40 wt % of the total Pu.
- A coating zone with an intermediate content of 7.3 hma % Pu, corresponding to 45 wt % of the total Pu.

These different Pu content zones are not present in equal quantities in the fuel; Talip et al. [24] estimated by Raman spectroscopy and EPMA analysis surface fractions of 46.7 %, 42.2 % and 11.1 % for the  $\rm UO_2$  matrix, the coating zone and the Pu agglomerates respectively.

Further characterisations and additional information on a similar MIMAS-MOX pellet with 7.48 wt. % Pu can be found in [6,15,23].

The MOX pellets were polished using 2400 grit SiC sandpaper prior to experiments. Before the introduction in the autoclave, the MOX fuel pellet was annealed for 5 h in a high temperature graphite furnace (Thermal Technology 1000–2560-FP20), located inside an inert atmosphere glove box. The annealing was carried out in Ar+5 %  $\rm H_2$  at 1200  $^{\circ}$ C, with a 20  $^{\rm O}$ C/min heating and cooling rate to remove any surface oxidation layer of the pellet formed during its long-term storage. Muzeau et al. [25] have shown that an oxidized surface layer forms on alpha doped materials during storage and the oxidation is proportional to their activity level.

The composition of the 3.27~mm half pellet was recalculated in August 2023 with a new specific alpha activity of 1.79~GBq/g before the start of the leaching test in the presence of metallic iron and simulated Forsmark groundwater and a new annealing was carried out before introduction in the autoclave.

## 2.1.2. Iron foils

Iron foils with  $\geq 99.99$  % purity (Thermo Scientific Alfa Aesar) of  $\sim 0.1$  mm thickness and  $\sim \! 1.56$  cm² surface area weighing 0.125 g were used in this experiment. The iron foils were polished with a #1200 grit (FEPA-P) Sic sandpaper in an inert-gas glovebox atmosphere to remove any pre-oxidized layer prior to the experiments. Iron foils were used in this present study to simulate the presence of iron, a major component of the canister material under a deep geological repository. The iron foil was rinsed in ethanol and ultrasound cleaned for a few minutes before use in the autoclave 2 g of iron powder (10  $\mu m, \geq 99.9$  % metal basis (Sigma -Aldrich, Merck) was also added to the autoclave for the leaching experiment.

#### 2.1.3. Autoclaves

For leaching under Ar atmosphere, a modified Parr 4760 pressure vessel with total internal volume  $0.5\ L$  (240 mL solution at start) was used in the experiments in the absence of iron.

A custom-made glass vessel eliminated any contact of the leaching solution with metallic parts of the autoclave. The original stainless steel dip tube was changed to a PEEK dip tube in order to be able to measure  $\rm H_2O_2$  concentrations.

A customized and modified Parr 4760 Stainless steel pressure vessel (Parr Instrument Co.) with a total internal volume of 1 L, which can withstand pressures of 131 bar and temperatures of 350 °C was used for the leaching experiments in presence of iron. The autoclave is equipped with two valves on the lid which allow for sampling of liquids and purging of gases. The original NPT (National Pipe Thread) lid connections were replaced with Swagelok VCR (Vacuum Coupling Radiation) connections to make the system more leak tight. During anoxic iron corrosion hydrogen is formed and it is important that the autoclave is tight for H<sub>2</sub>, which is much more difficult than for Ar. The autoclave is also equipped with a precision digital manometer with protective rubber cap (WIKA, CPG 1500 model) which allows to monitor the autoclave pressure during the entire experiment. Parr graphite gaskets (covered in a thin layer of silicon grease) were placed in the lid groove, which deforms when tightening the screws of the autoclave lid to create a gas tight seal. The graphite gasket is not to be reused in a new experiment. The autoclave experiment was conducted with a fitted glass beaker insert, so that the leaching solution was only in contact with the beaker, MOX fuel pellet, metallic iron foils, iron powder and the sampling dip

The synthetic Forsmark groundwater used for the experiment (see Section 2.2) was transferred into the glass beaker and purged with Ar gas for several hours before inserting into the autoclave. The autoclave containing the solution, and the materials used in this experiment was closed in a bench vise with a bolt-torque of 40 Nm, to ensure an even pressure of the bolts. The autoclave was then bubbled with Ar gas through the dip tube connection prior to the experiment start to flush the headspace, remove any traces of O<sub>2</sub>, and to saturate the solution with Ar. This process continued while the autoclave bolts were tightened in a crosswise fashion to ensure the absence of leakage before sufficient graphite gasket deformation had been achieved. The autoclave was equipped with custom-made PEEK dip tubes produced in the workshop, used for liquid sampling during the experiment.

Table 1
Composition and dimensions of the used 10 wt. % MIMAS-MOX pellets.

Oxide composition			Pu/Am isotopic composition				Dimen	sions	
UO <sub>2</sub>	PuO <sub>2</sub>	$AmO_2$	June 2019				Diameter	Height	
89.20 wt. %	10.17 wt. %	0. 63 wt. %	<sup>238</sup> Pu <sup>239</sup> Pu <sup>240</sup> Pu <sup>241</sup> Pu <sup>242</sup> Pu <sup>241</sup> Am		5.05 % 0.12 %	26.60 % 2.54 %	8.08 mm	3.27	7 mm

## 2.2. Synthetic groundwater compositions

For the experiments under only Ar, the solutions are a simplified groundwater model consisting of 10 mM NaCl and 2 mM NaHCO<sub>3</sub> prepared from ACS reagent grade chemicals (Sigma Aldrich  $\geq$  99.9 %).

The synthetic Forsmark groundwater solution used in experiments with Fe(s) was prepared using  $\geq 99.0$  % ACS reagent grade chemicals (Sigma-Aldrich, Merck) in ultrapure water having a resistivity of 18.2  $M\Omega.cm$  (MilliQ Advantage, Merck). A representative synthetic groundwater, as analyzed at the Forsmark site in Sweden [26,27] was prepared with the concentrations as given in Table 2. The amounts of chemicals used in its production are given in the Supplementary Material.

## 2.3. Experimental leaching procedure

## 2.3.1. Leaching in carbonated water (10 mM NaCl, 2 mM NaHCO<sub>3</sub> solution)

The autoclave solutions were bubbled with Ar gas prior to the experiment start to saturate the solution and remove any traces of  $\rm O_2$  which simultaneously flushed the headspace thoroughly during tightening of the screws. In each sampling, roughly 5 mL was sampled and discarded in order to rinse the dip tube and the connection in the autoclave lid. 3 mL samples were then taken, which were centrifuged in 23,300 rpm for 20 min to separate potential particles from the rest of the solution. Uncentrifuged samples were also analyzed, which allowed for potential identification of particles.

## 2.3.2. Leaching in Forsmark groundwater in presence of Fe(s)

The leaching experiment was carried out at ambient temperature (21.0  $\pm$  2.0 °C) under Ar atmosphere using an autoclave. The leaching autoclave reactor was airtight to assure anoxic conditions. The autoclave was sparged to eliminate residual air and pressurized to  $\sim$  10 bars with 99.96 % Ar + 0.04 % CO $_2$ . An 800 ml initial solution containing synthetic Forsmark groundwater as described in Section 2.2 was used in this experiment. The pressure of the autoclave was monitored throughout the experiment using a digital manometer.

The iron foil was cut into 2 strips and suspended in the autoclave filled with synthetic groundwater. Additionally, 2 g of iron powder in a small beaker was also added to the bottom of the autoclave. The metallic iron foils were slightly curved to enable maximum contact with water and easier identification of the foil surfaces. The iron foils and the iron powder were pre-corroded in 800 ml of synthetic Forsmark groundwater in the absence of the MOX fuel pellet. for a duration of 101 days. This step was taken to increase Fe(II) concentration in solution before MOX pellet introduction. The evolution of both Fe(II) concentrations and  $\rm H_2$  pressure was monitored during this preliminary step by taking solution samples at various time intervals and monitoring the pressure increase after each sampling during the whole duration of the experiment.

After the iron pre-corrosion stage, the autoclave was opened to introduce the unirradiated MIMAS-MOX pellet. The autoclave was opened in a plastic glove bag filled with Ar-gas. The annealed MOX fuel was placed at the bottom of the autoclave containing synthetic Forsmark ground water. The autoclave was then closed again, purged as before and pressurized to  $\sim 10$  bars with Ar+0.04 % CO2. Samples of the leaching solution were regularly collected over time and the pressure increase after each sampling was monitored with the manometer. The un-irradiated MOX leaching test with solution samplings at time intervals of about 30 days was continued for about one year.

Samples were collected without opening the autoclave through a liquid sampling valve, thanks to the overpressure inside the autoclave.

The leaching solution was regularly sampled over time. About 10 -  $12\,ml$  of the liquid was withdrawn from the sampling line at each time interval. The first aliquot (4–5 ml) taken at each sampling time was discarded prior to sampling in order to rinse the dip tube and the connection to the autoclave lid. Sample solutions of 6–7 ml were then taken for analysis. All sample solutions analysed throughout the experiment were filtered using 0.45  $\mu m$  syringe filter.

For the MOX leaching test, an extra separation step was carried out for the last few samplings in which the samples solutions were filtered using a syringe filter and  $0.20\,\mu m$  polypropylene membrane and Amicon Ultra-4 centrifugal filters with 30 kDa molecular weight cut-off, about 4 nm pore size (NMWL Sigma Aldrich Merck, Millipore Ltd) to evaluate the presence of any particulate matter or colloids.

## 2.4. Termination of the leaching experiment in presence of iron

At the end of the MOX leaching experiment, the autoclave was opened under Ar atmosphere in a glove bag. The MOX fuel pellet and the corroded iron foils and were retrieved from the solution, dried on Kimtech wipes and stored under argon atmosphere in the glove box until surface characterizations were carried out. The small beaker with iron powder was also retrieved and the iron powder separated by filtration. The leaching solution was filtered with a glass funnel and filter paper to separate any Fe powder from the solution, after which the volume of the filtered leaching solution was determined. The empty glass beaker was filled with 800 ml 0.5 M HNO3 and left for 24 h in order to release the uranium sorbed on the walls of the glass beaker. After the acidification, the glass beaker was emptied, then filled with 800 ml of 2 M HNO3 and left for another 24 h. Finally, the glass beaker was rinsed with ultrapure water. Solution samples were taken and analyzed for each acidification and rinse to quantify the total U sorbed or precipitated on the glass beaker.

The iron powder collected on the filter paper was dissolved in 2 M  $\rm HNO_3$  and the resulting solution was analyzed for U. After surface characterization of the iron foils, they were dissolved in 100 ml of 2 M  $\rm HNO_3$  for 24 h to quantify any U sorbed or precipitated on the iron foils. A sample of the solution was taken and analyzed by ICP-MS.

## 2.5. Solution analysis

## 2.5.1. pH and Eh

The pH of the solution samples taken from the autoclave with Forsmark groundwater was measured at different time intervals using a combined glass pH electrode calibrated against pH buffers. The electrode was calibrated with pH buffers of pH 1 (HCl), 4 (biphtalate), 7 (phosphate) and 10 (KCl /  $\rm H_3BO_3$  /NaOH) from Sigma Aldrich.

The Phenomenal ORP 220 redox electrode was used to determine the redox potential of the sampled solution. The redox electrode was calibrated using Mettler Toledo Inlab Redox Buffer solution (220 mV/pH7).

## 2.5.2. ICP-OES and mass spectrometry (ICP-MS)

Solution concentrations were determined using both ICP-OES (Inductively Coupled Plasma Optical-Emission Spectroscopy) (Thermo Scientific, Model iCAP Pro) and ICP-MS (Inductively Coupled Plasma Mass Spectrometry) instrument (Thermo Scientific, Model iCAP Q). In the preliminary iron corrosion study, ICP-OES was used to measure the total concentration of Fe(II) in solution. Before analysis, all filtered sample solutions were diluted with 0.5 M HNO<sub>3</sub> (Suprapur, Merck) containing 1 ppm Y as an internal standard (from 1000-ppm certified standard elemental stock solutions (CPAchem)). The dilution was

 $\label{thm:continuous} \textbf{Table 2} \\ \textbf{Chemical compositions of synthetic groundwaters. Concentrations in mmol/L.}$ 

ID	Na	K	Ca	Mg	$HCO_3$	Cl	$SO_4$	Si	Br	Fe(II)	Sr	pН
02A	96.57	0.93	22.21	10.04	2.07	148.9	5.28	0.22	0.3	0.04	0.1	7.19

necessary to enable the measured concentration within the linear range of the calibration. External calibration series of the analyzed elements were prepared from 1000 ppm, certified Fe standard stock solution (CPAchem) in the range of 0.325 to 20 ppm. The detection limit of the ICP-OES instrument was 0.1 ppm for Fe. The ICP-OES instrument is not conditioned for measuring radioactive solutions, and for this reason Fe concentrations in samples taken after introduction of the MOX pellet were measured by ICP-MS.

For the unirradiated MOX leaching test with synthetic Forsmark groundwater and metallic iron, ICP-MS was used to measure the total concentration of U, Pu and Fe. Both U and Pu concentrations were measured in the standard modes (STD) and solution samples were diluted with 0.5 M HNO3 (Suprapur, Merck) containing 2 ppb Bi-209 as an internal standard (from a 10-ppm certified standard stock solution (CPAchem)). External calibration series were prepared from 10 ppm, certified standard U stock solution (CPAchem) in the range of 0 - 50 ppb. The measurements of the Fe concentration from the sample solutions were performed using kinetic energy discrimination (KED) mode to be able to discriminate iron from polyatomic ion interferences [28]. The filtered sample solutions samples were diluted with 0.5 M HNO<sub>3</sub> (Suprapur, Merck) containing 2 ppb Y as an internal standard (from a 10-ppm certified standard stock solution (CPAchem). External calibration series were prepared from 10 ppm, certified Fe standard stock solution (CPAchem) in the range of 0 – 200 ppb.

All solution samples were analyzed in triplicates for total concentration determination with both instruments. Measurement uncertainties were found to be quite insignificant (<2 % relative uncertainty) for any concentrations above 0.1 ppb, due to the high resolution or detection limits of the ICP instrument. The uncertainties were not plotted in the concentration series since they overlap considerably with the datapoints. The detection limit for U and Pu is 0.1 ppb and for Fe is 1 ppb for the ICP-MS instrument.

## 2.5.3. $H_2O_2$ measurements in 10:2 solutions

The  $H_2O_2$ -concentrations were measured spectrophotometrically at 350 nm wavelength with a Shimadzu UV-1800 using the tri-iodide method based on the rapid oxidation of iodide in the presence of a molybdate catalyst [29–31] (Ghormley method). The spectrophotometer was calibrated using a 30 wt %  $H_2O_2$  solution (Sigma-Aldrich). 2 mL of the samples were mixed with 100  $\mu$ L 1 M KI ( $\geq$ 99.5 %, Sigma-Aldrich in MilliQ water) and 100  $\mu$ L ammonium molybdate tetrahydrate ( $\geq$ 99.0 %, Sigma-Aldrich) in an acetate buffer solution (pH 4.65, Sigma-Aldrich).

## 2.5.4. Alpha spectrometry

The specific activity of Pu was determined using an alpha spectrometer (Ortec, Alpha Duo, Octete-PC) equipped with low background, cooled passivated ion-implanted planar silicon (PIPS) detectors with an active area of 450 mm². Samples were placed 20 mm from the detector in the measurement chamber at a pressure of 0.05 to 1 mbar. Prior to measurement, the samples were diluted in 0.5 M HNO<sub>3</sub> at a dilution factor of 5 to prevent salt formation from the evaporation of the microsolution on the planchet, which could hinder alpha particles detection due to attenuation in the salt layer. The diluted solution was then transferred onto planchet, dried under an infrared lamp and further heated with an open flame (gas torch) to remove residual organic matter before insertion into the detector chamber. The instrument's detection limit was 0.1 Bq. mL¹

## 2.6. Surface analysis for the leaching in presence of iron

## 2.6.1. Scanning electron microscopy (SEM-EDX)

Two microscopes were used during this study. A Hitachi TM 3000 tabletop scanning electron microscope coupled with an energy-dispersive X-ray (EDX) was used for analysis of the MOX pellet surface. The Hitachi SEM was positioned in a glove box with argon

atmosphere. A Quanta 200 ESEM FEG scanning electron microscope (SEM) equipped with a Schottky field emission gun (FEG) for optimal spatial resolution was used to analyze the iron foils. The Quanta 200 ESEM microscope is also equipped with an Oxford Inca Energy Dispersive X-ray (EDX) system for chemical analysis of iron foils. The instruments were both operated in high vacuum mode (HV) and operating voltage of 30 kV. The iron foils were allowed to dry in an Ar atmospheric chamber glove box. The dried iron foils were deposited onto carbon tape. The iron foils were analyzed to determine the microstructure and elemental composition. The EDX spectra for the iron foils were measured at different locations.

For the MOX pellet, due to the activity of the pellet, it was analyzed using the SEM-EDX located inside the glove box. Due to the low resolution of the SEM-EDX in the glove box and uncalibrated EDX detector, the precipitates or deposits on the surface of the leached MOX fuel pellet were obtained by pressing Kapton tape on the pellet surface and detaching or peeling off the tape. This resulted in the presence of a visible red deposit on the surface of the Kapton tape. The detached sample on the Kapton tape was encapsulated in a sealed transport vessel to prevent contamination before analysis with the Quanta 200 ESEM FEG scanning electron microscope.

## 2.6.2. Raman spectroscopy

The WITec alpha300 R confocal Raman microscope with a cooled back-illuminated EMCCD detector was used to identify the secondary phases or precipitates formed on the surface of the iron foils and deposits from the MOX pellet surface. Samples were observed through an optical lens with a magnification of x100, with laser excitation of 532 nm and laser power of 0.6 mW was selected to avoid any oxidation of the samples under the beam.

## 2.6.3. Powder X-ray diffraction (P-XRD)

Even though XRD is a bulk solid method, it is listed here because X-ray diffraction analysis was performed on the red iron oxide deposit on the MOX pellet surface. The data were obtained using a BRUKER D2 PHASER instrument equipped with a monochromatic Cu K $\alpha$  lines ( $\lambda 1=1.54184~\mbox{\normalfont A}$ ) radiation source covering a  $2\Theta$  range from  $20^\circ$  to  $90^\circ$  and a LYNXEYE detector. The instrument was operated at a voltage of 30 kV and a current of 10 mA. Diffrac. Topas (V6.0) software provided by Bruker, in addition to the open access JEdit software [32], were used to determine the phases and crystal structure. The instrument was stationed or kept in the glove box with concentration of  $O_2 \leq 1$  ppm. The deposited samples from the MOX fuel pellet surface were analyzed for phase identification and crystal structure.

## 3. Results

## 3.1. Results of leaching in carbonated water

The evolution of the uranium concentrations during the leaching of the MOX pellet in 10 mM NaCl, 2 mM NaHCO $_3$  solution is shown in Fig. 2, together with the data for leaching in Forsmark water in the presence of Fe(s). Several leaching tests were carried out under only Ar and carbonated water, with similar results and only results from one are reported in the figure.

The  $\rm H_2O_2$  concentrations determined using the Ghormley method for the 10 wt. % Pu-doped MOX pellet, 10 bar Ar atmosphere experiment with PEEK dip tube were above detection limit (2  $10^{-6}$  M) after about 164 days and after 297 days reached a steady state concentration of 2. 6  $10^{-5}$  M (see Fig 1). All  $\rm H_2O_2$  concentrations were below detection limit in experiments with the stainless-steel dip tubes (not reported here), indicating that reactions with the dip tube caused a significant consumption of  $\rm H_2O_2$ .

As discussed in Section 2.1.1. the unirradiated MIMAS MOX fuel has a very complex structure concerning the distribution of Pu. This affects both the intensity of the alpha radiation in different locations of the

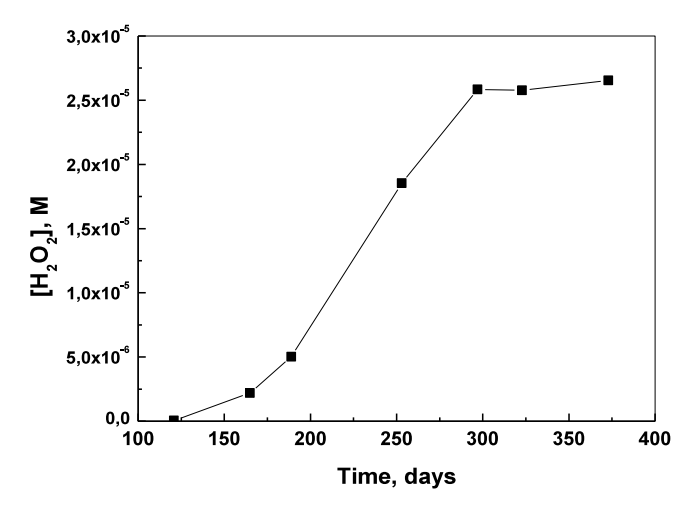


Fig. 1. Evolution of measured  $\rm H_2O_2$  concentrations with time for the 10wt % Pu MOX pellet under Ar atmosphere and PEEK dip tube experiment.

surface and the ease of its oxidative dissolution. Thus, locations with high Pu content are more difficult to dissolve [33,34], since Pu atoms do not get oxidized at valences higher than four in solid state. In the calculations presented here in the following, it is impossible to represent accurately this Pu distribution, instead an average dose rate is calculated assuming Pu evenly distributed in the  $\rm UO_2$  matrix.

The  $H_2O_2$  production rates of the 10 wt. % Pu-doped MOX pellets were modelled using the ASTAR stopping power data and the iterative attenuation approach [35]. Taking the surface area of the 10 wt. % Pu-doped MOX pellet into account, the  $H_2O_2$  production rate is  $3.46\cdot 10^{-8}$  mol·d<sup>-1</sup>.

Only  $\alpha$ -radiation is considered in the dose rate and  $H_2O_2$  production rate calculation, as both  $\beta$  and  $\gamma$  dose rates are orders of magnitude lower for unirradiated MOX fuels [7,15,36].

The uranium release rate is rather low during the first 20 days, but around the 30–40 days mark, the releases reach a steady value, at about  $2.4\ 10^{-7}\ \text{mol}\cdot\text{d}^{-1}$ .

As seen from Fig. 2, the concentration of U increases steadily during the whole duration of the test. The plutonium concentrations could be measured only at the first two samplings ( $\sim 2~10^{-8}$  M) and decreased later below detection limit ( $< 10^{-10}$  M).

## 3.2. Results for the MOX leaching experiment in presence of iron

The pH of the solution, measured in the presence of iron both before

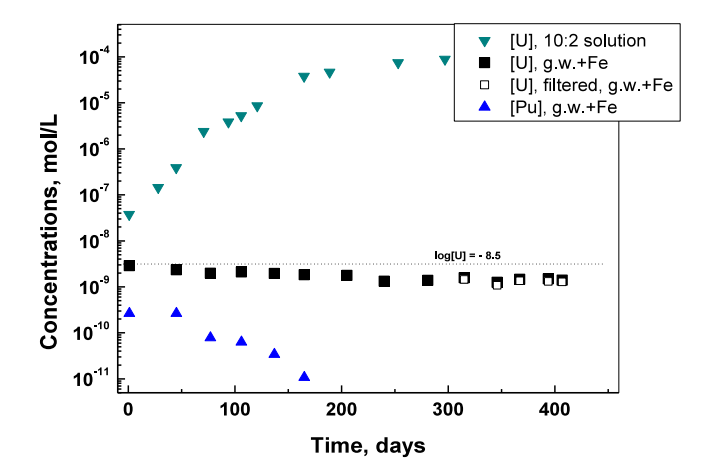


**Fig. 2.** Evolution of U and Pu concentrations in solution during leaching of the 10 wt % Pu MOX pellet under Ar in 10 mM NaCl, 2 mM NaHCO<sub>3</sub> solution and in Forsmark groundwater in presence of Fe(s).

and after introduction of the MOX pellet, ranged from 6.9 ( $\pm$  0.1) to 7.2 ( $\pm$  0.1), with no notable changes observed throughout the duration of the leaching experiment. Redox potential (E<sub>h</sub>) measurements were conducted on the sampled solutions towards the end of the MOX leaching experiment yielding values between -30 and -40 mV/SHE. While these measurements showed some instability, they all correspond to reducing conditions even though they were carried out in air atmosphere. This is consistent with the expectations that iron corrosion releases redox-active species such as Fe<sup>2+</sup> and H<sub>2</sub> that create reducing conditions in the solution. The Pt redox electrode is sensitive both to the Fe(II)/Fe(III) couple and to H<sub>2</sub>/H<sup>+</sup> couple, hence a small drift towards more positive potentials was noted during measurements in air atmosphere due to both a decrease of Fe(II) concentrations given its fast reaction with O2 of air and the decrease of H2 concentrations due to degassing. Only minor decreases were observed for the concentrations of most groundwater components, given the high solution to solid ratio in our experiment.

Uranium concentrations in solution were measured using ICP-MS, while the plutonium concentrations were measured by both ICP-MS and alpha spectrometry. Both U and Pu concentrations in solution were followed as they could be an indicator of the oxidative dissolution of the MOX pellet. The measured dissolved plutonium concentrations were, with exception for a few initial data points, under the detection limits of the ICP-MS instrument throughout the entire duration of the experiment. Likewise, the activities measured by the alpha-spectrometry and alpha counting were less than the detection limits of the instrument (0.1 Bq. mL<sup>-1</sup>), thereby limiting the ability to measure and quantify the Pu activity or content in the synthetic Forsmark ground water solutions.

The measured concentrations for uranium in the leaching experiment are shown in Fig. 1. The U concentrations which are at start 0.7  $\mu g/L$  (2.9  $\times$   $10^{-9}$  M) gradually decrease to 0.3  $\mu g/L$  after 240 days of leaching. This concentration remains almost the same until the end of the experiment (407 days), indicating that a steady state concentration has been reached.

The low initial concentration of U observed in this study suggests that the pre-oxidized surface layer of the pellet was effectively minimized or prevented which would have otherwise resulted in a higher initial U concentration. The consistently low U concentrations measured throughout the experiments indicate a significant influence of groundwater chemistry and the presence of metallic iron. For the few filtered and ultrafiltered samples (samples from 315 days and on) collected towards the end of the experiment, the U concentration remained almost the same suggesting that the formation of colloids was unlikely.

The presence of dissolved Fe(II) in the solution and generation of hydrogen, both of which are reducing species, plays a significant role in inhibiting or suppressing the oxidative dissolution of the MOX fuel. The alpha activity of the MOX pellet is anticipated to induce alpha radiolysis of water leading to the formation of oxidizing species such as  $\rm H_2O_2$ . Based on the low and slightly decreasing with time uranium concentrations, which are in good agreement with lower limit of the solubility of UO $_2$  (am,hyd) [2], indicating that uranium is present as U(IV) in solution, the 10wt % Pu MIMAS-MOX pellet was therefore not submitted to oxidative dissolution by radiolytic species.

The plutonium concentrations were below detection limit for alpha spectrometry (0.1 Bq/mL) and the ICP-MS data reported in Fig. 1 are quite low, however they are about an order of magnitude higher than the solubility of PuO<sub>2</sub>(am, hyd) based on the values selected in [2]. They are however quite similar to the Pu concentrations reported by Rai et al. [37] for the reductive dissolution of PuO<sub>2</sub>(am,hyd) in the presence of 1 mM Fe(II). The standard reduction potential of the Fe(III)/Fe(II) couple (E $_0 = 0.772$  V, [38]) is much lower than this of the Pu(IV)/Pu(III) couple (E $_0 = 1.047$  V, [2]), hence Fe(II) is expected to reduce Pu(IV) to Pu(III) in solution. As discussed in Section 3.6.1, there is a massive Fe(OH)<sub>3</sub>(s) production at the surface of the MOX pellet due to radiolytic oxidation of Fe(II), besides this produced by Pu(IV) reduction and sorption of plutonium to these newly formed surfaces may be an explanation for the

decreasing concentrations below detection limit also for ICP-MS.

# 3.3. Analysis of distribution of U in aqueous solution and sorbed/precipitated on solid surfaces

To quantify the total uranium released in the system containing both iron foil and iron powder, the uranium distribution across various system components was assessed at the conclusion of the leaching experiment. Fig. 3 illustrates the partitioning of uranium into soluble fractions, sorbed or precipitated fractions on the quartz beaker insert within the autoclave reactor, and onto the surfaces of the corrosion products on iron foil and iron powder. The soluble uranium fraction accounted for only 1.2 % of the total uranium released corresponding to 0.14 µg. Approximately 4.9 % (0.58 µg) was found on the iron foils. The fraction sorbed or precipitated on the quartz beaker insert represents 10.4 % (1.24 µg). The majority of the released uranium was retained within the iron powder amounting to 83.5 % (9.91 µg), which had also the largest surface in contact with the solution. Overall, a total of 11.9 µg of uranium was mobilized in the presence of metallic iron after a leaching duration exceeding one year. This very low amount of uranium mobilized during the more than one-year long test indicates that it was mainly sorbed U(IV) on the various surfaces.

## 3.4. Iron concentrations in solution

The concentrations of Fe(II) in solution were measured at different time intervals using ICP-OES before introducing the MOX pellet and by ICP-MS after pellet introduction. The evolution of the iron concentration in solution is reported in Fig. 4. The measured Fe concentration increases initially almost linearly with time, confirming the corrosion of the metallic iron foils in contact with the synthetic groundwater. The anoxic corrosion of the iron is expected to produce Fe(II) in solution and hydrogen pressure, as shown in Eq. (1). After 101 days, the autoclave was opened to introduce the MOX pellet and a slight decrease of Fe(II) concentration was caused by the unavoidable oxygen contamination, even though the autoclave was opened in a glove bag. It is anticipated that Fe(II) as a potential aqueous reducing species could influence the dissolution behaviour of the MOX fuel to be introduced into the autoclave during the MOX leaching experiment. Relatively high Fe(II) concentrations have been demonstrated in similar studies to suppress the oxidative dissolution of the fuel [13–15].

As seen from Fig. 4, the Fe concentrations increase almost linearly

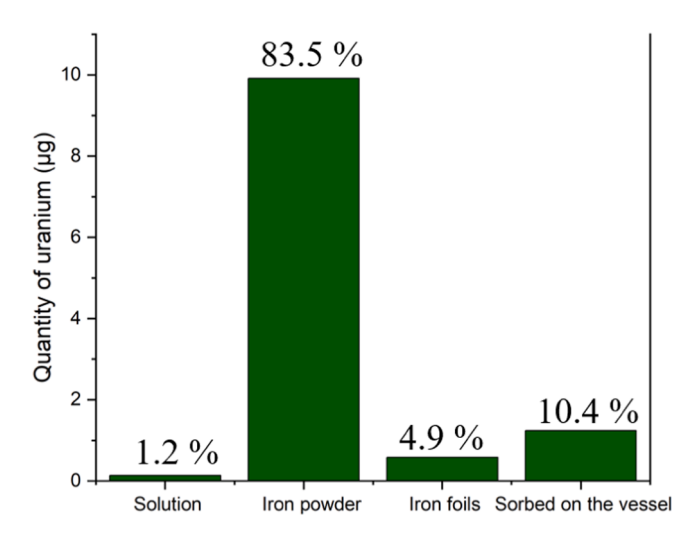


**Fig. 3.** Uranium distribution among solution, iron powder, iron foils, and the sorbed/precipitated fraction on the glass beaker insert as evaluated at the conclusion of the MOX leaching experiment in synthetic Forsmark groundwater in the presence Fe(s).

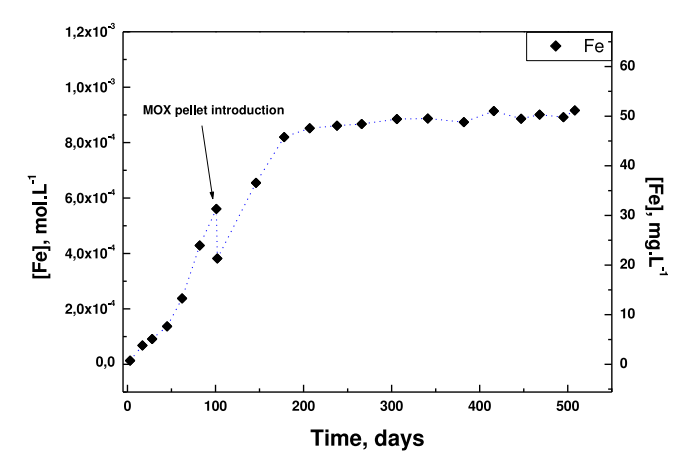


**Fig. 4.** Evolution of dissolved Fe concentrations in solution during leaching of the MOX pellet in Forsmark synthetic groundwater.

during the initial stage of the leaching experiment. After approximately 150 days, the Fe levels seem to stabilize, reaching a plateau at around 48–50 mg/L. This stabilization suggests the formation of iron secondary phase precipitates with relatively high solubility.

## 3.5. Hydrogen evolution

Fig. 5 shows the changes in hydrogen pressure in the presence of metallic iron both before and after introducing the MOX fuel pellet.

During the initial 101 days, corresponding to the pre-iron corrosion phase, a gradual increase in hydrogen pressure was observed with an average hydrogen production rate of 7.2  $10^{-5}$  mol  $\rm H_2/day$ . After introducing the MOX fuel pellet into the experiment, the monitoring of  $\rm H_2$  pressure continued until the end of the 508-day leaching period.

The average hydrogen generation rate in the active autoclave is  $8.6.10^{-5}$  mol  $\mathrm{H_2/day}$ , i.e. slightly higher than in the absence of the MOX pellet. The observed  $\mathrm{H_2}$  production rate in the active autoclave is quite similar to that reported in [9], who observed a  $\mathrm{H_2}$  production rate of  $8.5.10^{-5}$  mol  $\mathrm{H_2/day}$  for the leaching experiment of spent fuel in the presence of iron powder over 1250 days.

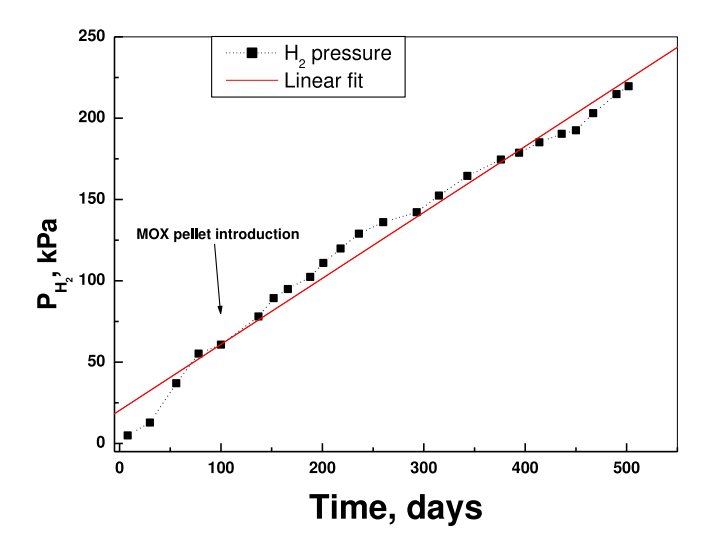


Fig. 5. Evolution of the hydrogen pressure in the autoclave.

3.6. Results of surface characterizations of the MOX fuel pellet and iron foils

3.6.1. SEM-EDX analysis of the iron oxide precipitate on MOX fuel pellet

The surface of the MOX pellet at the end of the leaching test was
completely covered by a several µm thick red precipitate with granular
shape, see Fig. 6.

The first SEM micrographs of the surface of the unirradiated MOX pellet leached in synthetic Forsmark groundwater in the presence of iron were acquired in a Hitachi TM 3000 tabletop SEM, which had an uncalibrated EDX detector, hence only micrographs were obtained, see Fig. 7.

The EDX analyses of the granules and the corresponding mappings realized on the precipitates formed on the surface of the MOX pellet were obtained by pressing Kapton tape on the surface of the pellet and analyzing the powder attached on the tape. The EDX spectrum and the mapping are shown in Fig 8. The SEM-EDX analysis suggests that the precipitates primarily consist of Fe containing compounds, which formed at the fuel/ water interface through the oxidation of Fe(II) to Fe (III). Previous studies on alpha-doped UO<sub>2</sub> pellet have shown that iron hydroxides such as akageneite ( $\beta$ -FeOOH) tend to precipitate on the surface of leached MOX pellet in the presence of iron [13–15].

The EDX analysis performed (see Fig. 8) shows Fe and O as the major elements in the compounds formed, with trace amounts of Si, C, Ca, Na, S, Cl and Mn, most likely originating from evaporation of synthetic groundwater (average of EDX analyses performed on 11 different areas or spots). However, no traces of uranium were observed in any of the spectra.

3.6.2. Powder XRD analysis of the red deposit on the MOX pellet surface

The X-ray diffraction analysis performed on the red deposit or precipitate sample aimed to characterize its structural phases. The resulting diffractogram did not reveal distinct peaks, indicating the presence of amorphous phases. The XRD pattern shows broad peaks and not well-defined peaks as shown in Fig. 9. The precipitates formed on the surface of the pellet are mainly amorphous and the presence of microcrystallinity cannot be ruled out. The diffractogram was compared against the ICDD database for indexing, yielding matches with some peaks for a variety of Fe(III) oxides such as lepidocrocite, goethite, akageneite, hematite and maghemite. In any case, as seen from Fig. 9, all these compounds are mainly amorphous, and we could not determine any crystalline compounds with certainty.

# 3.6.3. Raman spectroscopy analysis of the precipitates on the surface of MOX pellet

Raman spectroscopy was conducted on the precipitate that formed

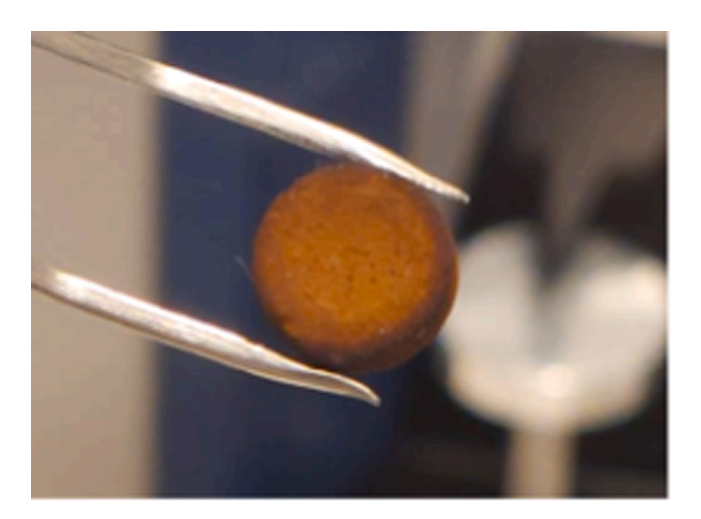


Fig. 6. Picture of the MOX pellet when extracted from the autoclave.

on the surface of the MOX pellet to characterize the nature of precipitate formed. The resulting Raman spectrum, displayed in Fig. 10, right which is derived from analyses of six distinct areas or spots was compared to the spectrum of akageneite ( $\beta$ -FeOOH) as reported in [39]. Similar peaks have also been observed in the study of Odorowski et al. [13]and Jegou et al. [15]. The spectrum in Fig. 10, left has similarities with Raman spectrum of lepidocrocite ( $\gamma$ -FeOOH) as reported in [40] with observed peaks at 248, 303.392,654 and 1312 cm<sup>-1</sup>. The Raman spectra of akageneite ( $\beta$ -FeOOH) and lepidocrocite ( $\gamma$ -FeOOH) exhibit characteristic peaks corresponding to their iron oxyhydroxide structures, with their vibrational modes associated with Fe-O-Fe bending and Fe-O stretching or bending vibrations, as well as Fe-O-H bending modes influenced also by hydrogen bonding and crystal symmetry [41–46].

The findings from this study and other existing literature suggest that the precipitates formed on the surface of the MOX pellet are composed of a variety of Fe(III) oxides such as goethite, akageneite, lepidocrocite etc. formed through oxidation of Fe(III) to Fe(III) by reaction with  $\rm H_2O_2$  and other radiolytic oxidants.

## 3.6.4. SEM-EDX analyses on the corroded iron foils

The surfaces of the iron foils were also observed by SEM-EDX at the end of the leaching experiment. Fig. 11 shows the micrographs of the corroded iron foil taken at different areas and magnification. The micrographs show that the iron foils corroded during the leaching experiment comprise different phases. Precipitation of nano to micro metric particles is observed on the corroded iron foils.

The EDX analysis performed on different micrographs (average of EDX analyses on  $8{\text -}10$  different areas or spots on each micrograph analyzed) of the corroded iron foils show that the precipitates contain  $85{\text -}90$  at. % Fe with the remaining  $10{\text -}15$  at. % consisting of O, Ca, Si, C and Cl, with traces of Na, Mn, Mo also present mostly likely from the ground water evaporation. The elemental compositions are shown in Fig. 12. Out of the total 82 EDX analysed performed on different areas of the micrographs, only one micrograph shows traces of U (1 at. %), associated with other elements from the groundwater composition such as Si, S, Fe, Cl,  $O_2$  and Mo. This is very probably due to the drying of leaching solution containing groundwater components and dissolved U (IV)

Mapping analyses were also carried out on the corroded iron foils at different mapping areas or regions (13 different mapped areas). They show similar compositions consisting of Fe, O, Ca and Si. A full mapping scan of an area of the corroded iron foil is shown in Fig. 13.

Based on the SEM-EDX analysis, iron corrosion products such as Fe (II) hydroxide, Fe(II) hydroxy-carbonates as well as calcite seem most likely to form, since O, H and C are not easily detectable by EDX being lighter elements.

## 3.6.5. Raman spectroscopy analyses of the corroded iron foils

The Raman shifts observed on the precipitates from the corroded iron foils are primarily dominated by peaks at  $1084-1086~{\rm cm}^{-1}$ , and  $713-716~{\rm cm}^{-1}$  with additional smaller peaks at  $277-280~{\rm cm}^{-1}$  and  $154-155~{\rm cm}^{-1}$ , as shown in Fig. 14. These peaks are in good agreement with the spectrum of ankerite (CaFe<sup>II</sup> (CO<sub>3</sub>)<sub>2</sub>)) as reported in [13,47] and from the RRUFF database (RRUFF online database, ID number R050197). In some spots, the obtained spectra are similar to the spectrum of calcite (CaCO<sub>3</sub>) from the RRUFF database, particularly the peaks at 280 and 1086 cm<sup>-1</sup> (RRUFF online database, ID number R050127). Some features in Fig. 11c and 11d seem to have some similarity with chukanovite morphology, but it was difficult to find those spots with the Raman microscope.

Raman spectra obtained from some spots on the foils show the presence of a dominant peak at  $218 \, \mathrm{cm}^{-1}$  along with other smaller peaks as shown in Fig 15. Peaks were observed at approximately 165, 218, 306, 386, 529, and 647 cm<sup>-1</sup>. This spectrum is identical to that of cronstedtite Fe<sub>2</sub><sup>2+</sup>Fe<sup>3+</sup>(Si, Fe<sup>3+</sup>O<sub>5</sub>)(OH)<sub>4</sub> as referenced in the RRUFF database (RRUFF online database, ID number R061026). The Raman

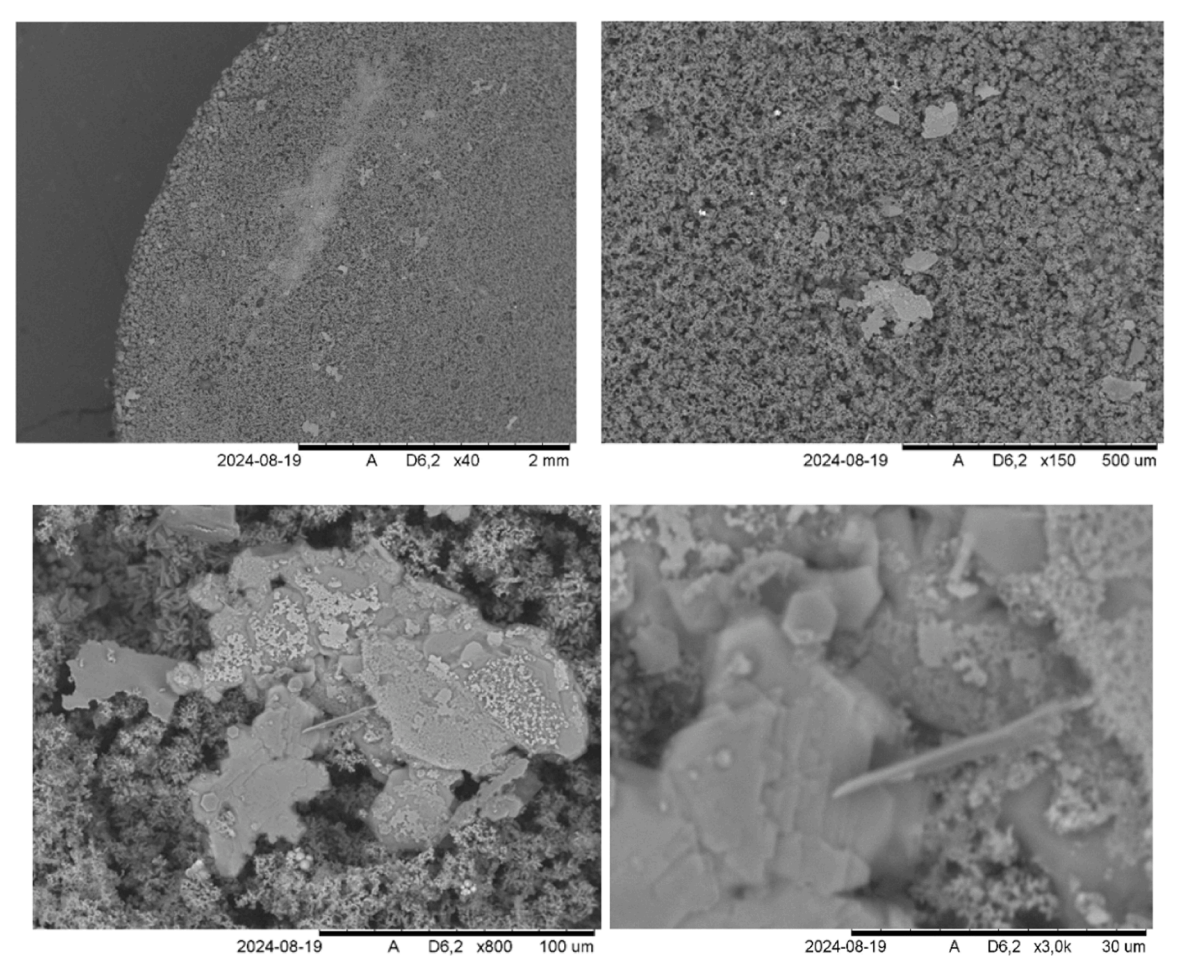


Fig. 7. SEM micrographs of the leached MOX pellet in synthetic Forsmark groundwater in the presence of iron.

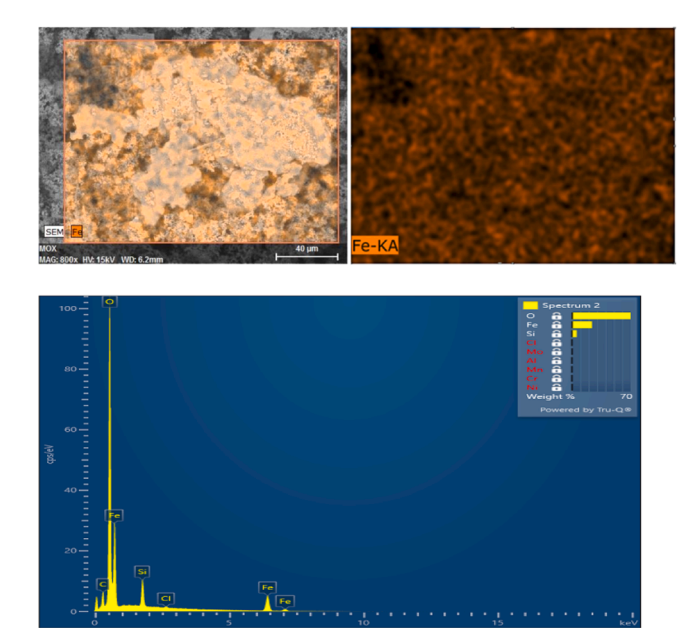


Fig. 8. Mapping and EDX analyses of the precipitates formed on the leached MOX pellet surface.

spectrum of cronstedtite exhibits several distinct bands that reflect its layered phyllosilicate structure. Peaks were observed at approximately165, 218, 306, 386, 529, and 647 cm<sup>-1</sup>, with the dominant peak

centred at 218 cm $^{-1}$ . These peaks most likely correspond to vibrational modes characteristic of Fe-rich phyllosilicates with 1:1 layered structures [48,49]. The band near 165 cm $^{-1}$  likely arises from combined Fe–O and Si–O sheet motions. From broader phyllosilicate reviews, the  $\sim$ 200–250 cm $^{-1}$  region correspond to lattice vibration modes involving the layer framework [50]. The major peak at 218 cm $^{-1}$  can be attributed primarily to Fe–O octahedral lattice vibrations. While direct Raman spectral data on cronstedtite remain limited, the observed Raman bands in cronstedtite align well with vibration mode analyses of related phyllosilicate and layered silicates proposed in [50], allowing for plausible mode labeling despite the absence of studies that directly assign each band to specific Fe–O or Si–O vibrations in cronstedtite

Additionally, EDX analyses and elemental mappings of the precipitates from the corroded iron foils confirmed the presence of Fe, O and Si within the precipitates.

The Raman measurement results, combined with EDX elemental composition analysis, suggest that the precipitates formed on the surface of the corroded iron foils are most likely ankerite and calcite. However, the potential formation of phases such as cronstedtite and chukanovite cannot be excluded.

## 4. Discussion

During the leaching experiments in carbonated water (10 mM NaCl, 2 mM NaHCO $_3$  solution) the extensive hydrogen peroxide production by the strong alpha radiation of the MOX pellet causes the oxidation of U (IV) atoms of the surface to U(VI) which is then extracted in solution as uranyl carbonate complexes.

During the leaching in presence of iron, only slight changes in the pH  $\,$ 

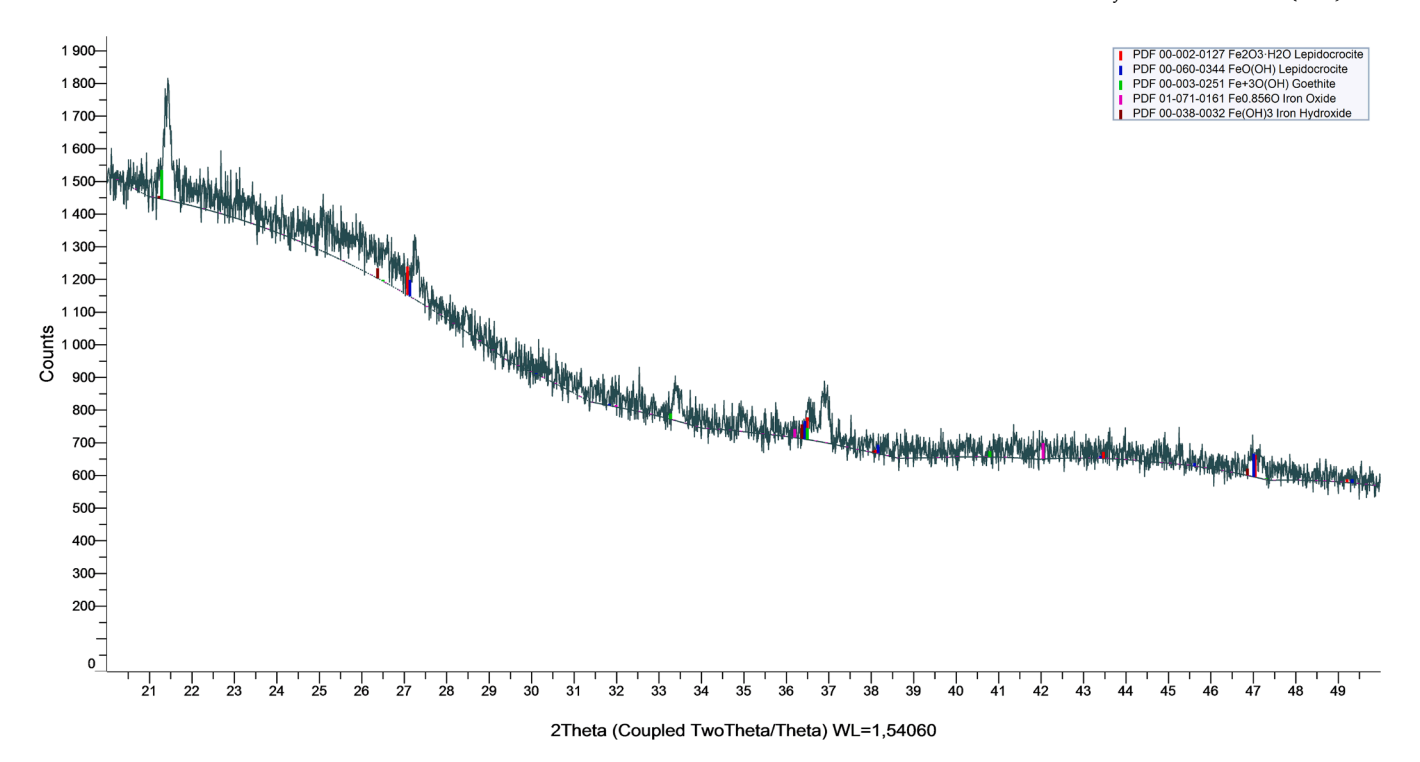


Fig. 9. XRD patterns of the red deposit or precipitates formed on the surface of the leached MOX pellet. The sharper peaks originate from Kapton tape and sample holder.

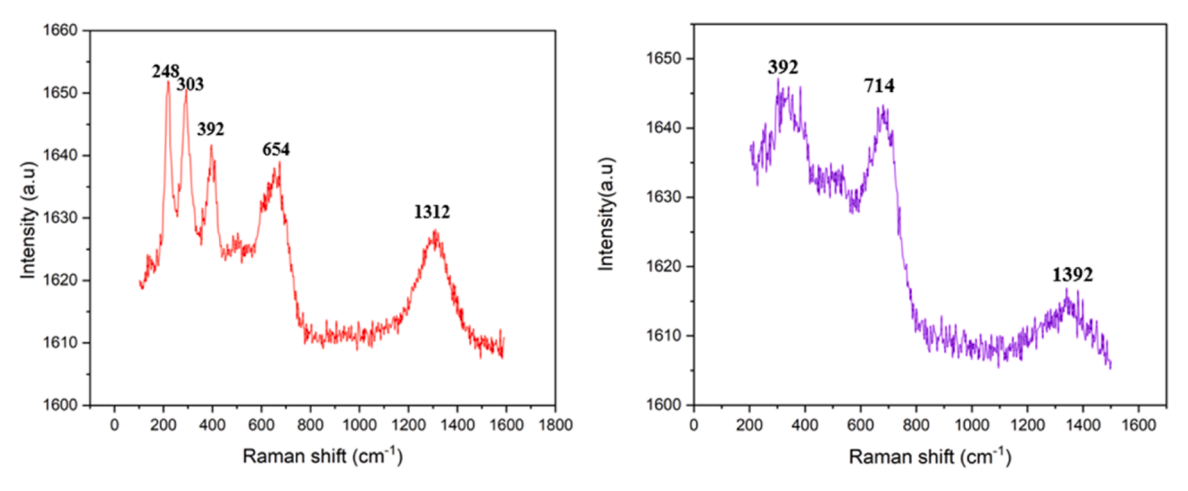


Fig. 10. Raman spectra of the precipitates found on the leached MOX pellet.

and composition of the groundwater were observed during the test while the Eh values measured in the samples taken from the autoclave in the presence of air were still negative. This can be partially due to the relatively high hydrogen concentrations produced during the long test, which means that the real redox potential is higher than the measured value (hydrogen is active on the Pt redox electrode, but not in the bulk solution). A slight decrease of the Ca concentration (but not e.g. Sr) in the groundwater was observed, which together with other observations (e.g. the similar C and Ca areas in the mappings shown in Fig 13) indicate that calcite precipitation occurred during the more than one-year long test. This has been observed before [51,52] for simulated Allard groundwater compositions calculated in equilibrium with calcite at the corresponding depth and slight changes of the  $\rm CO_2$  partial pressure can cause calcite precipitation.

Anyhow, the major influence of groundwater is in the corrosion mechanism of the metallic iron. Magnetite was not detected in corrosion products, as was the case for iron corrosion in 10 mM NaCl, 2 mM

NaHCO<sub>3</sub> solution [9,10] and very probably much more soluble Fe (II) hydroxy carbonates such as chukanovite or double layered carbonate green rust has been formed as corrosion products. The relatively high and quite constant Fe(II) concentrations (8.5-9.2  $\times$  10<sup>-4</sup> M) from 200 days on in our experiment indicate for the potential presence of a very soluble Fe(II) phase. In other cases [13,14] even higher Fe(II) concentrations are reported. Very probably such a Fe(II) phase is highly amorphous and hence probably difficult to observe and characterize, alternatively the active iron corrosion creates the surplus of Fe(II) ions. This is because the reported concentrations of Fe(II) in equilibrium synthetized siderite [53] or chukanovite [54,55] are more than an order of magnitude lower, i.e. about 10<sup>-5</sup> M. Calculations with Phreege C and Thermochimie database indicate that Fe(II) concentrations slightly lower  $(4.5 \times 10^{-4} \text{ M})$  instead of  $9.2 \times 10^{-4} \text{ M}$ ) than those measured in our test can be achieved by equilibration of Forsmark groundwater with chukanovite.

It is interesting to note that a slight acceleration of the iron corrosion

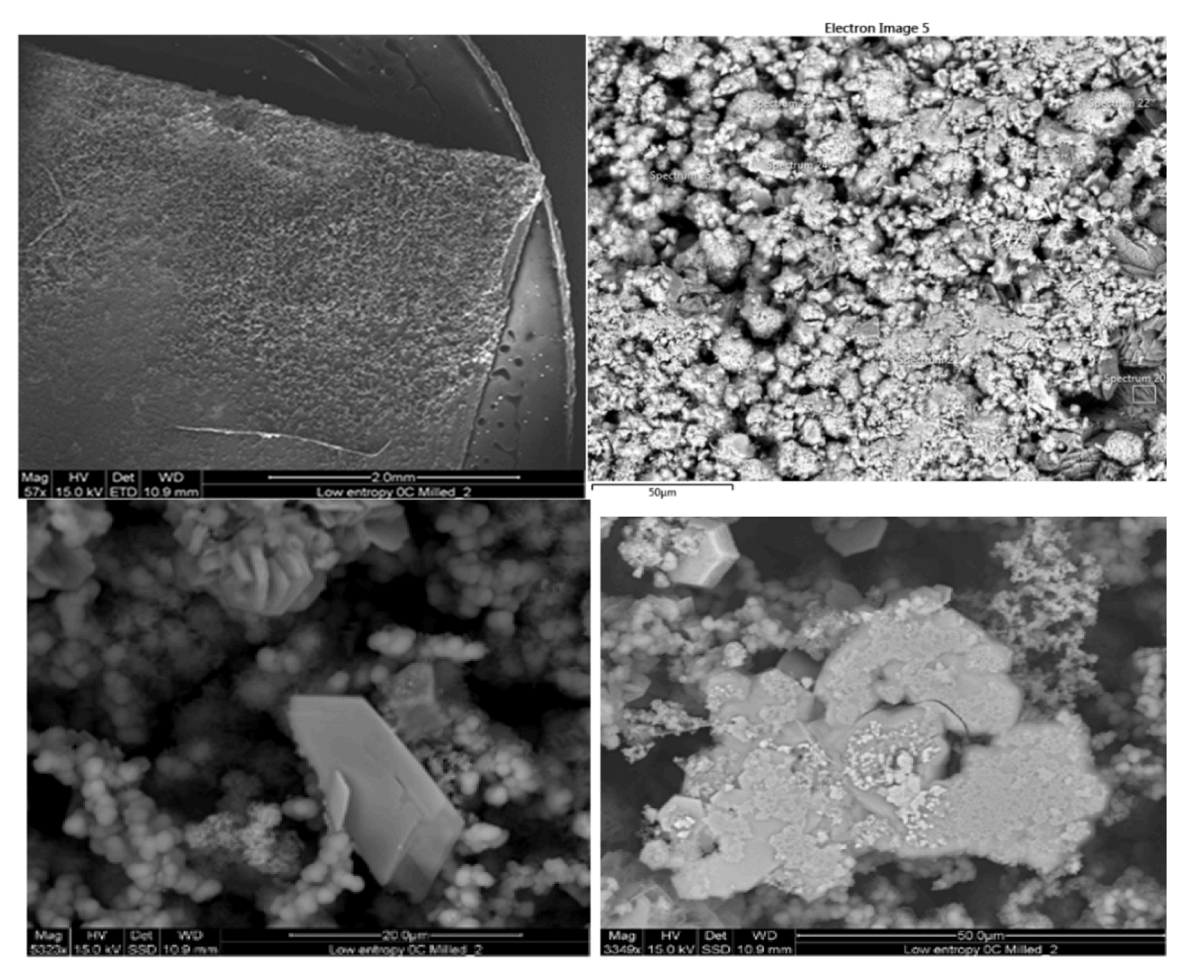


Fig. 11. (a-d). SEM- micrographs of the corroded iron foils.

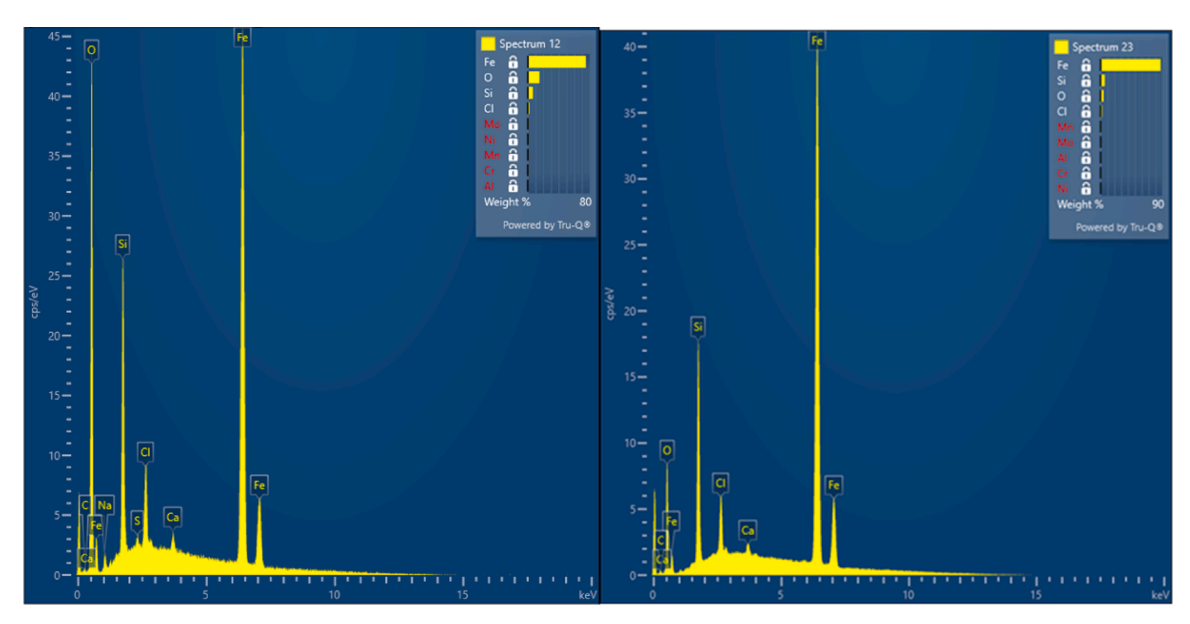


Fig. 12. SEM-EDX spectrum on the corroded iron foils.

was observed even in the case of an unirradiated MOX pellet, namely the hydrogen production was slightly higher in the presence of the pellet as compared to the initial corrosion phase in its absence. The radiolytically produced hydrogen is orders of magnitude lower and cannot explain this increase. This acceleration of corrosion was first noted by Smart et al.

[56] during iron corrosion in the presence of spent nuclear fuel and confirmed later by Puranen et al. [9] also for iron corrosion in the presence of spent fuel.

During the whole leaching period of  $>\!400$  days there are no signs of increase of the uranium concentrations, instead a slight decrease is

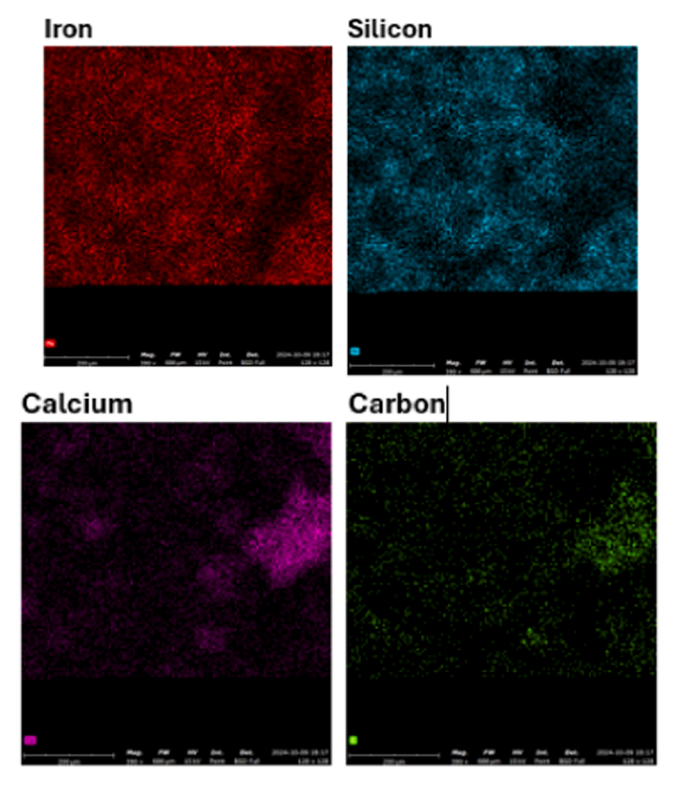


Fig. 13. Mapping of the corroded iron foils.

noted. As discussed in [57], these low U concentrations cannot be due to equilibrium with any U(VI) solid phase, because even the most insoluble uranyl silicates, such as soddyite and uranophane, have solubilities which are at least 100 times higher than the ones measured in our test. Calculations with Phreeqe C and Thermochimie V.12 SIT database show U concentrations in equilibrium with Forsmark groundwater of 2.8  $10^{-4}$  M for soddyite (UO<sub>2</sub>)<sub>2</sub>SiO<sub>4</sub>.2H<sub>2</sub>O and 2  $\times$  10<sup>-4</sup> M for uranophane Ca (UO<sub>2</sub>)<sub>2</sub>(SiO<sub>3</sub>OH)<sub>2</sub>.5H<sub>2</sub>O including the Ca-uranyl-carbonate complexes. Without these ternary complexes, the concentrations of U for soddyite and uranophane in equilibrium with Forsmark groundwater are respectively 9.4  $\times$  10<sup>-5</sup> M and 6.3  $\times$  10<sup>-6</sup> M.

The measured uranium concentrations during the whole duration of the test in presence of iron are in excellent agreement with the lower limit of the solubility of UO<sub>2</sub>(am, hyd) in this pH range, log [U]= $-8.5\pm1$ , as selected in NEA TDB [2]. The absence of any traces of U(VI) in solution is confirmed also by the absence of any traces of U in the

SEM-EDX of the red precipitate taken from the surface of the MOX pellet or on the surface of the iron foils.

It is well known and confirmed in several studies of ZVI (Zero Valent Iron) barriers [58–63] and studies in the radwaste community [11,12, 64,65] that traces of U(VI) are reduced and precipitate as  $UO_2(s)$  on the surface of corroding metallic iron.

It has been shown that Fe(II) in solution does not reduce uranyl but does reduce it when sorbed in various surfaces including Fe(III) oxides [66]. Du et al. [67] have argued that the reduction can occur at pH and  $E_h$  conditions at which  $\Delta G$  results negative, assuming that one mole of the one electron reductant Fe(II) can reduce in homogeneous solution half a mole of U(VI) to UO\_2(s), a process which requires two electrons for each uranyl ion.

Any U(VI) which would diffuse from the fuel surface out would be reduced in the Fe(III) oxides deposited on the pellet by Fe(II) ions. If U (VI) makes it to the iron foils or iron powder a few centimeters away from the pellet, it will be reduced and deposited on the iron surface as  $UO_2(s)$  [11,12]. This is apparently not the case, because both EDX analysis of the red precipitate and of the iron foils show no signs of U accumulation.

Further, the analysis of the uranium distribution between different surfaces shows very small amounts deposited on metallic iron, quite consistent with the strong sorption of U(IV) on iron corrosion products

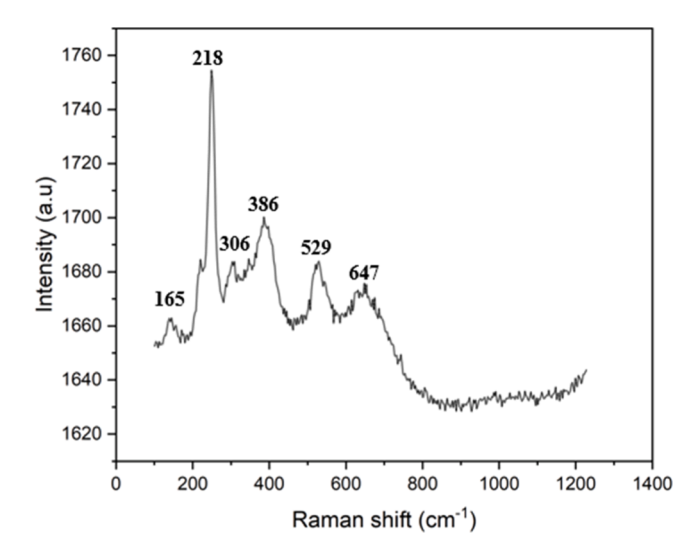


**Fig. 15.** Raman spectra of the precipitates found on the surface of the corroded iron foils.

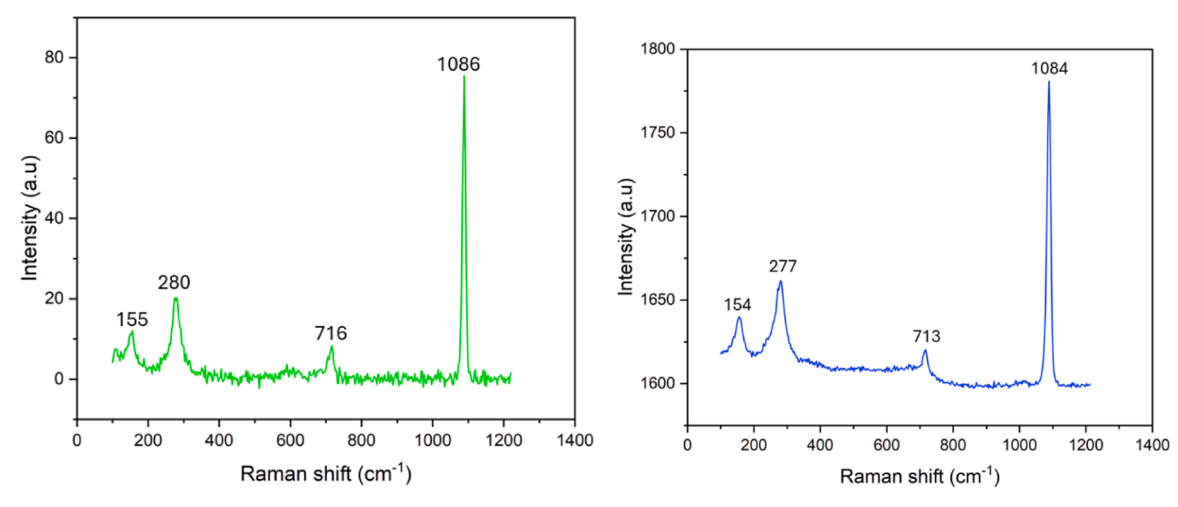


Fig. 14. Raman spectra of the precipitates found on the surface of the corroded iron foils.

[9,68,69]. The  $K_d$  value calculated for uranium sorption on the corroded part of the metallic powder (using the same approach as in [9]) is 24.4 m³/kg, while  $K_d$  for sorption in the metallic foils is 11. 4 m³/kg. These values agree well with those reported in [9] and with published values for sorption of actinide ions on iron corrosion products [68]. The fraction of uranium sorbed on the glass vessel (10.4 %) agrees quite well with the reported value for sorption of Th(IV) on borosilicate glass vials at near neutral pH [70].

Any escape of  $H_2O_2$  from the about 40  $\mu m$  layer near the pellet where it is produced by  $\alpha$ -radiolysis can be dismissed because it would cause oxidation and precipitation of Fe(III) oxides in the bulk solution and the solutions were clear at the end of the test. Another argument is the low and constant U concentrations measured, which would increase if  $H_2O_2$  reaches bulk solution due to its very fast reaction with U(IV) in solution [71,72].

As discussed before in [9,15], the two potential reductants which cause these effects are Fe(II) ions in solution and dissolved hydrogen. Fe (II) reacts with hydrogen peroxide relatively fast in two steps. In the first step Fe(III), an OH-ion and an OH-radical are produced:

$$Fe(II) + H_2O_2 \rightleftarrows Fe(III) + OH^{-} + OH \bullet$$
(3)

This reaction is relatively fast, the reported rate constants  $k_3$  vary between 40 and 80  $M^{-1}s^{-1}$  [73]. The OH-radial produced in this reaction oxidizes very fast ( $k_4=3.2\ 10^8\ M^{-1}s^{-1}$ , [74]) another Fe(II) ion, so the summary reaction is:

$$2 \text{ Fe(II)} + \text{H}_2\text{O}_2 \rightleftarrows 2 \text{ Fe(III)} + 2 \text{ OH}^- \tag{4}$$

Dissolved molecular hydrogen produced by iron corrosion does not react with  $H_2O_2$ , but can react fast with the OH-radical produced in the first step of  $H_2O_2$  reaction with Fe(II):

$$OH' + H_2 \rightarrow H_2O + H'$$
 (5)

In this process a very reducing radical, atomic hydrogen, is produced which can reduce fast hydrogen peroxide, other radiolytic oxidants or oxidized uranium. As noted by Jegou et al. [15] the reaction of the OH radical with Fe(II) is slightly faster than its reaction with hydrogen, but the overall rate of the reaction depends both on the kinetic constant and on the concentration of the reactant. In our test the hydrogen pressure reached ~2 bars, corresponding to ~1.6 mM dissolved hydrogen and this higher concentration may compensate for the smaller kinetic constant. A third factor to consider is the presence of carbonate in our groundwater solutions, which converts the OH-radical to a carbonate radical, also a very strong oxidant. The OH-radical produced in reaction (3) can be scavenged also by Cl<sup>-</sup> and Br<sup>-</sup> present in the groundwater, with rate constants which are higher than these for reaction with H<sub>2</sub> or Fe(II), while H<sub>2</sub>O<sub>2</sub> may also be catalytically decomposed into two surface adsorbed OH-radicals on surfaces such as UO2(s) or spent fuel doped with various amounts of fission products.

All these homogeneous reaction pathways for radiolytic hydrogen peroxide reaction with Fe(II) should be compared with its reaction with the solid UO<sub>2</sub>(s) surface. It has been shown that radiation induced oxidation of UO<sub>2</sub> is completely dominated by H<sub>2</sub>O<sub>2</sub> (> 99 %) in  $\alpha$ -irradiated systems [75]. Hydrogen peroxide both oxidizes the surface and is decomposed to water and oxygen. In a relatively recent study [76], it was shown that these two competing reactions share a common intermediate and therefore occur at the same surface site [77].

The mechanism is described by the following reactions and kinetic constants:

$$H_2O_2 + 2 UO_2 \rightarrow 2 HO^{\bullet} UO_2$$
 (ks1)

$$H_2O_2 + HO^{\bullet} - UO_2 \rightarrow HO_2^{\bullet} + H_2O + UO_2$$
 (ks2)

$$HO_2^{\bullet} + HO_2^{\bullet} \rightarrow H_2O_2 + O_2 \tag{ks3}$$

$$HO^{\bullet}-UO_2 \to OH^- + UO_2^+$$
 (ks4)

Given the complexity of this mechanism, it is not possible to experimentally assess the rate constants of the elementary reactions separately from each other. However, on the basis of experiments performed at different initial concentrations of  $\rm H_2O_2$  at a given solid surface to solution volume ratio where the concentrations of  $\rm H_2O_2$  and dissolved uranium were monitored as a function of time, the individual rate constants could be assessed using numerical fitting to the mechanism [78]. It should be noted that the constant for the reaction between two  $\rm HO_2$  radicals producing  $\rm H_2O_2$  and  $\rm O_2$  is already known and therefore does not require fitting. Based on fitting to experimental data, the rate constants were determined to ks1 = 0.462 M $^{-1}$  s $^{-1}$ , ks2 = 0.191 s $^{-1}$ , ks3 = 197 M $^{-1}$  s $^{-1}$  and ks4 = 34.1 M $^{-1}$  s $^{-1}$ .

A comparison of ks1 and ks4 values for reactions of  $H_2O_2$  with  $UO_2(s)$  surface with the constants  $k_3$  and  $k_4$  for its reaction with Fe(II) ions, shows that the reactions with Fe(II) are much faster. This may be a possible explanation for the inhibition of the oxidative fuel dissolution by relatively large concentrations of Fe(II) ions.

## 5. Conclusions and outlook

The corrosion of an unirradiated MOX fuel pellet containing 10 wt % Pu (specific alpha activity  $1.79~\mathrm{GBq/g}$ ) was investigated under Ar atmosphere in carbonated water (2 mM NaHCO<sub>3</sub>,  $10~\mathrm{mM}$  NaCl) and in simulated granitic groundwater from Forsmark, Sweden in the presence of metallic iron foils and iron powder. The U(VI) release in the simplified  $10.2~\mathrm{solution}$  was proportional to the alpha radiation field of the pellet which produced  $H_2O_2$  and other radiolytic oxidants at the pellet surface.

The results of the test in the presence of iron show that the anoxic corrosion products of iron neutralized completely the high alpha field of the MOX pellet. The production of hydrogen continued during the whole test with a linear rate of 8.5 10<sup>-5</sup> mol H<sub>2</sub>/day, reaching about 2 bars H<sub>2</sub> pressure at test termination. The Fe(II) concentrations increased from 5.6 10<sup>-4</sup> M after 101 days and MOX pellet insertion to 9.2 10<sup>-4</sup> M at test termination. No traces of oxidized uranium were observed in the autoclave during the whole duration (407 days) of the test, the uranium concentrations (from 2.9 10<sup>-9</sup> M at start to 1.2 10<sup>-9</sup> at the end) are in good agreement with the lower range of  $UO_2(am)$  solubility. Massive Fe (III) precipitation was observed on the surface of the MOX pellet, but not in the bulk solution. The Pu concentrations were below the detection limit of alpha spectrometry. Very low Pu concentrations were measured only at the initial stage of the leaching as determined by ICP-MS, later Pu was under detection limit even for this method. The analysis of the iron foils, iron powder and vessel surfaces showed that the majority of U(IV) was sorbed on iron corrosion products and much less in the glass surfaces of the vessel. Anoxic iron corrosion products such as ankerite were detected on the iron foils while several Fe(III) compounds including goethite, lepidocrocite and akageneite were formed on the surface of the MOX pellet. Our study shows that the anoxic corrosion of iron in granitic Forsmark groundwaters completely blocks the oxidative dissolution of a MOX pellet with a very high specific alpha activity.

In order to understand better if dissolved hydrogen has any influence in the process, it is desirable to synthetize Fe(II) compounds which can produce similar high Fe(II) concentrations as those measured in our autoclave and test the leaching of the MOX pellet in the presence of such compounds.

## CRediT authorship contribution statement

M. Saleh: Writing – review & editing, Writing – original draft, Methodology, Investigation, Formal analysis, Data curation, Conceptualization. N.L. Hansson: Writing – review & editing, Methodology, Investigation, Formal analysis. M. Hedberg: Writing – review & editing, Writing – original draft, Investigation, Formal analysis. K. Spahiu: Writing – review & editing, Supervision, Methodology, Formal analysis, Conceptualization. C. Ekberg: Writing – review & editing, Supervision, Funding acquisition, Conceptualization.

## Declaration of competing interest

The authors declare that they have no known competing financial interests or personal relationships that could have appeared to influence the work reported in this paper.

#### Acknowledgements

The Swedish Nuclear and Fuel and Waste Management Company (SKB) is greatly acknowledged for funding of this research project. The authors wish to thank Christophe Jegou and especially Veronique Broudic of CEA, Marcoule for all their administrative work related to the transport of the MIMAS MOX pellet to Chalmers in 2018, which made this study possible.

## Supplementary materials

Supplementary material associated with this article can be found, in the online version, at doi:10.1016/j.jnucmat.2025.156202.

## Data availability

Data will be made available on request.

#### References

- D.W. Shoesmith, Fuel corrosion processes under waste disposal conditions, J. Nucl. Mater. 282 (2000) 1–30.
- [2] I. Grenthe, X. Gaona, A. Plyasunov, L. Rao, W.H. Runde, B. Grambow, R.J. M. Konings, A.L. Smith, E.E. Moore, Second Update on the Thermodynamics of U, Np, Pu, Am and Tc, OECD Nuclear Energy Agency Data Bank Eds., OECD publications, Paris, France, 2020.
- [3] J.W.T. Spinks, R.J. Woods, An Introduction to Radiation Chemistry, 3rd ed., John Wiley & Sons Inc, New York, 1990.
- [4] L. Liu, I. Neretnieks, The effect of hydrogen on oxidative dissolution of spent fuel, Nucl. Technol. 138 (2002) 69–77.
- [5] P. Sellin, SR 97: hydromechanical evolution in a defective canister, MRS Symp. Proc. 663 (2002) 755–763.
- [6] M. Odorowski, C. Jégou, L. De Windt, V. Broudic, S. Peuget, M. Magnin, M. Tribet, C. Martin, Oxidative dissolution of unirradiated MIMAS MOX fuel (U/Pu oxides) in carbonated water under oxic and anoxic conditions, J. Nucl. Mater. 468 (2016) 17, 25
- [7] V. Kerleguer, C. Jegou, L. De Windt, V. Brudic, G. Juan, S. Miro, F. Tocino, The mechanisms of alteration of a homogeneous U<sub>0, 73</sub>Pu<sub>0, 27</sub>O<sub>2</sub> MOX fuel under alpha radiolysis of water, J. Nucl. Mater. 529 (2020) 151920 paper.
- [8] P. Carbol, P. Fors, S. Van Winckel, K. Spahiu, Corrosion of irradiated MOX fuel in presence of dissolved H<sub>2</sub>, J. Nucl. Mater. 392 (2009) 45–54.
- [9] A. Puranen, A. Barreiro-Fidalgo, L.Z. Evins, K. Spahiu, Spent fuel corrosion and the impact of iron corrosion – The effects of hydrogen generation and formation of iron corrosion products, J. Nucl. Mater. 542 (2020) 152423 paper.
- [10] A. Puranen, A. Barreiro-Fidalgo, L.Z. Evins, K. Spahiu, Spent fuel leaching in the presence of corroding iron, MRS Adv., Energy Sustain. 2 (12) (2017) 681–686.
- [11] D. Cui, K. Spahiu, The reduction of U(VI) on corroded iron under anoxic groundwater conditions, Radiochim. Acta 90 (2002) 1–6.
- [12] N. Hansson, M. Saleh, P.L. Tam, S. Holgersson, K. Spahiu, C. Ekberg, Influence of groundwater composition on the reductive precipitation of U(VI) on corroding iron foil surfaces. J. Nucl. Mater. 577 (2023) 154324.
- [13] M. Odorowski, C. Jegou, L. de Windt, V. Broudic, G. Jouan, S. Peuget, C. Martin, Effect of metallic iron on the oxidative dissolution of UO<sub>2</sub> doped with a radioactive alpha emitters in synthetic Callovo-Oxfordian water, Geochim. Cosmochim. Acta 219 (2017) 1–21.
- [14] M. Odorowski, Etude de L'altération de la Matrice (U,Pu)O<sub>2</sub> du Combustible Irradié en Conditions de Stockage Géologique :Approche Expérimentale et Modélisation Géochimique, Ph. D. Thesis, Mines Paris Tech, France, 2015.
- [15] C. Jegou, M. Odorowski, V. Kerleguer, V. Broudic, M.L. Schlegel, G. Jouan, C. Marques, L. De Windt, MOX fuel corrosion processes under waste disposal conditions, J. Corr. Sci. 195 (2022) 109964.
- [16] M. Saheb, D. Neff, P. Dillmann, H. Matthiesen, E. Foy, Long-term corrosion behavior of low-carbon steel in anoxic environment: characterization of archaeological artefacts, J. Nucl. Mater. 379 (2008) 118–123.
- [17] J.-M. Genin, M. Abdelmoula, C. Ruby, C. Upadhyay, Speciation of iron; characterisation and structure of green rusts and Fe<sup>II-III</sup> oxyhydroxycarbonate fougerite, C. R. Geoscience 338 (2006) 402–419.
- [18] AM. C.Aissa Ruby, R. Géhin, J. Cortot, M. Abdelmoula, J.-M. Génin, Green rusts synthesis by coprecipitation of Fe(II)-Fe(III) ions and mass balance diagram C.R. Geosci. 338 (2006) 420–432.

- [19] N.R. Smart, D.J. Blackwood, L. Werme, Anaerobic corrosion of carbon steel and cast iron in artificial groundwaters: part 1-electrochemical aspects, Corrosion 58 (2002) 547–559.
- [20] N.R. Smart, D.J. Blackwood, L. Werme, Anaerobic corrosion of carbon steel and cast iron in artificial groundwaters: part 2-gas generation, Corrosion 58 (2002) 627–637.
- [21] N.R. Smart, A.P. Rance, L.O. Werme, Anaerobic corrosion of steel in bentonite, Mat. Res. Soc. Symp. Proc. 807 (2004) 441–446.
- [22] N.R. Smart, A.P. Rance, L. Carlson, L.O. Werme, Further studies of the anaerobic corrosion of steel in bentonite, MRS Symp. Proc 932 (2006) 813–820. V.
- [23] G. Oudinet, I. Munoz-Villard, L. Aufore, M.-J. Gotta, J.M. Becker, G. Chiarelli, R. Castelli, Characterization of plutonium distribution in MIMAS MOX by image analysis, J. Nucl. Mater. 275 (2008) 86–94.
- [24] Z. Talip, S. Peuget, M. Magnin, M. Tribet, C. Valot, R. Vauchy, C. Jegou, Characterization of un-irradiated MIMAS MOX fuel by Raman spectroscopy and EPMA, J. Nucl. Mater. 499 (2018) 88–97.
- [25] B. Muzeau, C. Jégou, F. Delaunay, V. Broudic, A. Brevet, H. Catalette, E. Simoni, C. Corbel, Radiolytic oxidation of UO<sub>2</sub> pellets doped with alpha emitters (<sup>238</sup>/<sub>239</sub>Pu), J. All. Comp. 467 (2009) 578–589.
- [26] M. Laaksoharju, J. Smellie, E.-L. Tullborg, M. Gimeno, J. Molinero, J. Gurban, L. Hallbeck, Hydrogeochemical evaluation and modelling performed within the Swedish site investigation programme, Appl. Geochem. (2008) 1761–1795.
- [27] M. Laaksoharju, J. Smellie, E.-L. Tullborg, M. Gimeno, L. Hallbeck, J. Molinero, N. Waber, Bedrock Hydrogeochemistry Forsmark. Site descriptive Modelling SDM-Site Forsmark, SKB R-08-47, Svensk Kärnbränslehantering AB, 2008.
- [28] N. Yamada, Kinetic energy discrimination in collision/reaction cell ICP-MS: theoretical review of principles and limitations, Spectrochim. Acta, Part B: Atom. Spectrosc. 110 (2015) 31–44.
- [29] A.O. Allen, C.J. Hochanadel, J.A. Ghormley, T.W. Davis, Decomposition of water and aqueous solutions under mixed fast neutron and γ-radiation, J. Phys. Chem. 56 (1952) 575–586.
- [30] C. Hochanadel, Effects of cobalt γ-radiation on water and aqueous solutions, J. Phys. Chem. 56 (1952) 587–594.
- [31] J. Ghormley, A. Stewart, Effects of  $\gamma$ -radiation on ice 1, J. Am. Chem. Soc. 78 (13) (1956) 2934–2939.
- [32] A. Klaver, JEdit: a text editor and more, Linux J. 2011 (209) (2011) 7. Iss.
- [33] C. Jegou, R. Caraballo, J. De Bonfils, V. Broudic, S. Peuget, T. Vercouter, D. Roudil, Oxidizing dissolution of spent MOX47 fuel subjected to water radiolysis: solution chemistry and surface characterization by Raman spectroscopy, J. Nucl. Mater. 399 (2010) 68–80.
- [34] C. Jegou, R. Caraballo, S. Peuget, D. Roudil, L. Desgranges, M. Magnin, Raman spectroscopy characterization of actinide oxides (U<sub>1,y</sub>Pu<sub>y</sub>)O<sub>2</sub>: resistance to oxidation by the laser beam and examination of defects, J. Nucl. Mater. 405 (2010) 235–243.
- [35] N. Hansson, M. Jonsson, C. Ekberg, K. Spahiu, Geometrical aspects of alpha dose rates for  $\rm UO_2$  based fuels, Radiat. Phys. Chem. 199 (2022) 110336 paper.
- [36] L. Bauhn, Ekberg Hansson, C. Fors, P. Delville, R. Spahiu, The interaction of molecular hydrogen with α-radiolytic oxidants on a (U,Pu)O<sub>2</sub> surface, J. Nucl. Mater. 505 (2018) 54–61.
- [37] D. Rai, Y.A. Gorby, J.K. Fredrickson, D.A. Moore, M. Yui, Reductive dissolution of PuO2(am): the effect of Fe(II) and hydroquinone, J. Soln. Chem. 31 (2002) 433–453.
- [38] R.J. Lemire, U. Berner, C. Musikas, D.A. Palmer, P. Taylor, O. Tochiyama, Chemical thermodynamics of iron. Part 1. OECD Nuclear Energy Agency Data Bank Eds, OECD Publications, Paris, France, 2013.
- [39] D. Neff, Apport Des Analogues Archéologiques a L'Estimation Des Vitesses Moyennes Et a L'Étude Des Mécanismes De Corrosion a Très Long Terme Des Aciers Non Alliés Dans Les Sols, Ph.D. Thesis, Université de Technologie de Compiègne, France, 2003.
- [40] D.J.A. De Faria, S.V. Silva, M.J. de Oliveira, Raman microspectroscopy of some iron oxides and hydroxides, J. Raman Spectrosc. 28 (1997) 873–876.
- [41] S.J. Oh, D.C. Cook, H.E. Townsend, Characterization of iron oxides commonly formed as corrosion products on steel, Hyperfine Interact. 112 (1998) 59–66.
- [42] J.E. Post, V.F. Buchwald, Crystal structure refinement of akaganeite, Am. Mineral. 76 (1991) 272–277.
- [43] W.R. Richmond, J.H. Hockridge, M. Loan, G.M. Parkinson, A new iron oxyhydroxide phase: the molybdate-substituted analogue of akaganeite, Chem. Mater. 16 (2004) 3203–3205.
- [44] D. Lewis, V. Farmer, Infrared-absorption of surface hydroxyl-groups and latticevibrations in lepidocrocite (gamma-FeOOH) and boehmite (gamma-AlOOH), Clay Miner. 21 (1986) 93–100.
- [45] B. Weckler, H.D. Lutz, Lattice vibration spectra. Part XCV. Infrared spectroscopic studies on the iron oxide hydroxides goethite, akagankite, lepidocrocite and feroxyhite, Eur. J. Solid State Inorg. Chem. 35 (1998) 531–544.
- [46] E.C. Sklute, S. Kashyap, M. Darby Dyar, J.F. Holden, T. Tague, P. Wang, S.J. Jaret, Spectral and morphological characteristics of synthetic nanophase iron oxyhydroxides, Phys. Chem Miner. 45 (1) (2018) 1–26.
- [47] M.L. Schlegel, C. Bataillon, F. Brucker, C. Blanc, D. Prêt, E. Foy, M. Chorro, Corrosion of metal iron in contact with anoxic clay at 90 degrees C: characterization of the corrosion products after two years of interaction, Appl. Geochem. 51 (2014) 1–14.
- [48] R.G. Burns, Mineralogical Applications of Crystal Field Theory, 2nd ed., Cambridge University Press, 1993.
- [49] V.C. Farmer, The layer silicates. The Infrared Spectra of Minerals, Mineralogical Society, 1974, pp. 331–343.

- [50] A. Wang, J.J. Freeman, B.L. Jolliff, Understanding the Raman spectral features of phyllosilicates, J. Raman Spectrosc. 46 (10) (2015) 829–845.
- [51] K. Spahiu, L. Werme, J. Low, U.-B. Eklund, In situ long term measurements of pH and redox potential during spent fuel leaching under stationary conditions the method and some preliminary results, MRS Symp. Series 608 (2000) 55–60.
- [52] Vuorinen, U. and Snellman, M., 1998. Finnish Reference Waters for Solubility, Sorption and Diffusion Studies, Posiva Working Report 98-61, Posiva Oy, Finland.
- [53] D. Cui, J. Low, K. Spahiu, Environmental behaviors of spent nuclear fuel and canister materials, Energy Environ. Sci. 4 (2011) 2537–2545.
- [54] R. Chen, J. Chen, M. Hong, W. Zhang, Formation of chukanovite in simulated groundwaters containing CO<sub>3</sub><sup>2</sup>, Environ. Technol. 37 (2016) 2786–2792.
- [55] T.R. Lee, R.T. Wilkin, Iron hydroxide carbonate formation in zerovalent iron permeable reactive barriers: characterization and evaluation of phase stability, J. Contam. Hydrol. 116 (2010) 47–57.
- [56] N.R. Smart, A.P. Rance, L.O. Werme, The effect of radiation on the anaerobic corrosion of steel, J. Nucl. Mater. 379 (2008) 97–104.
- [57] E. Ekeroth, M. Granfors, D. Schild, K. Spahiu, The effect of temperature and fuel surface area on spent nuclear fuel dissolution kinetics under H2 atmosphere, J. Nucl. Mater. 531 (2020) 151081 paper.
- [58] J.N. Fiedor, W.D. Bostick, R.J. Jarabek, J. Farrell, Understanding the mechanism of uranium removal from groundwater by zero-valent iron using X-ray photoelectron spectroscopy, Environ. Sci. Technol. 32 (1998) 1466–1473.
- [59] B. Gu, L. Liang, M.J. Dickey, X. Yin, S. Dai, Reductive precipitation of uranium (VI) by zero-valent iron, Environ. Sci. Technol. 32 (1998) 3366–3373.
- [60] J. Farrel, W.D. Bostick, R. Jarabek, N. Fiedor, Uranium removal from ground water using zero valent iron media, Ground Water 37 (1999) 618–624.
- [61] S.J. Morrison, D.R. Metzler, C.E. Carpenter, Uranium precipitation in a permeable reactive barrier by progressive irreversible dissolution of zero valent iron, Environ. Sci. Technol. 35 (2001) 385–390.
- [62] C R.A. Crane, M. Dickinson, I. Popescu, T.B. Scott, Magnetite and zero-valent iron nanoparticles for remediation of uranium contaminated environmental water, Water Res. 45 (2011). p.2391-2342.
- [63] R.A. Crane, M. Dickinson, T.B. Scott, Nanoscale zerovalent iron particles for the remediation of plutonium and uranium contaminated solutions, Chem. Eng. J. 262 (2015) 319–325.
- [64] B. Grambow, E. Smailos, H. Geckeis, R. Muller, H. Hentschel, Sorption and reduction of uranium (VI) on iron corrosion products under reducing saline conditions, Radiochim. Acta 74 (1996) 149–154.

- [65] M. Rovira, S.E. Amrani, L. Duro, J. Gimenez, J. de Pablo, J. Bruno, Interaction of uranium with in-situ anoxically generated magnetite on steel, J. Haz. Mat. 147 (2007) 726–731.
- [66] E. Liger, L. Charlet, P. Van Cappellen, Surface catalysis of uranium (VI) reduction by iron (II), Geochim. Cosmochim. Acta 63 (1999) 2939–2955.
- [67] X. Du, B. Boonchayaanant, W.-M. Wu, F. Scott, J. Bargar, C.G. Criddle, Reduction of uranium (VI) by soluble iron (II) conforms with thermodynamic predictions, Environ. Sci. Technol. 45 (2011) 4718–4725.
- [68] D. Li, D.I. Kaplan, Sorption coefficients and molecular mechanisms of Pu, U, Np, Am and Tc to Fe (hydr)oxides: a review, J. Haz. Mater. 243 (2012) 1–18.
- [69] I. Rojo, F. Seco, M. Rovira, J. Giménez, G. Cervantes, V. Martí, J. de Pablo, Thorium sorption onto magnetite and ferrihydrite under acidic conditions, J. Nucl. Mater. (2009) 474–478.
- [70] E. Maulden, D.E. Wall, N.A. Wall, Silanization for minimizing tracer cation sorption on glass vials, J. Radioanal. Nucl. Chem. 333 (2024) 4233–4241.
- [71] F.B. Baker, T.W. Newton, The reaction between U(IV) and hydrogen peroxide, J. Phys. Chem. 65 (1961) 1897–1899.
- [72] A.J. Elliot, S. Padamshi, J. Pika, Free radical redox reactions of uranium ions in sulphuric acid solutions, Can. J. Chem. 64 (1986) 314–320.
- [73] A. Fischbacher, C. von Sontag, T.C. Schmidt, Hydroxyl radical yields in Fenton process under various pH, ligand concentrations and hydrogen peroxide/Fe(II) ratios, Chemosphere 182 (2017) 738–744.
- [74] Z. Stuglik, Z.P. Zagorski, Pulse radiolysis of neutral iron(II) solutions: oxidation of ferrous ions by OH radicals, Rad. Phys. Chem. 17 (1981) 229–233.
- [75] E. Ekeroth, O. Roth, M. Jonsson, The relative impact of radiolysis products in radiation induced oxidative dissolution of UO2, J. Nucl. Mater. 355 (2006) 38–46.
- [76] A. Barreiro Fidalgo, Y. Kumagai, M. Jonsson, The role of surface-bound hydroxyl radicals in the reaction between H2O2 and UO2, J. Coord. Chem. 71 (2018) 1799–1807
- [77] Jonsson, M., 2024. Assessment of Heterogeneous Processes and Parameters to be Used in Models for Radiation Induced Spent Nuclear Fuel Dissolution, SKB Report R-23-12, Svensk Kärnbränslehatering AB.
- [78] N. Hansson, M. Jonsson, C. Ekberg, K. Spahiu, Modelling radiation-induced oxidative dissolution of UO<sub>2</sub>-based spent nuclear fuel on the basis of the hydroxyl mediated surface mechanism, J. Nucl. Mater. 578 (2023) 154369 paper.